POLITECNICO DI MILANO
Corso di Laurea MAGISTRALE in Ingegneria Biomedica
Dipartimento di Elettronica, Informazione e Bioingegneria



POLITECNICO
MILANO 1863

Advanced approaches for blood pressure regulation assessment. Application in a porcine model of cardiac arrest

B^3 Lab
Politecnico di Milano

Relatori: Ing. Manuela Ferrario
Prof. Giuseppe Baselli
Prof. Filippo Molinari

Tesi di Laurea di:
Mario Lavanga
matricola 813680

Anno Accademico 2014-2015

Nisi efficiamini sicut parvuli, non entrabitis in regnum caelorum
Matthew, the apostle

Se te resta el coeur me quell d'on fioeu, te sareè on grand òmm.
Anonymous writer of Lombardy region

Abstract

Previous studies proved that the baroreceptor reflex (baroreflex) control of heart rate can be used for stratification of post-infarction population and, in general, cardiovascular diseases populations. The baroreflex can be assessed by different methods either invasive, by means of pharmacological manoeuvre, or non-invasive, i.e. in spontaneous conditions. Those methods provide the baroreflex estimate known as baroreflex sensitivity (BRS) expressed as $ms/mmhg$. Most of the studies that exploits BRS are focused mainly on acute myocardial infarction (AMI) and there are no important literature works which investigate the role of BRS during and immediately after cardiac arrest (CA). The analysis of the CA effects on the BRS could provide further knowledge about the mechanisms involved in the CV system response and thus paves the way for a more effective treatment. The present work is a prosecution of the published work of Ristagno et al. (2014). In particular, the objectives of this thesis are (1) to study the evolution of BRS after CA and following CPR as in previous studies and to verify if the recovery of CV stability and arterial blood pressure is accompanied by a recovery of BRS values in porcine model; (2) to verify if the BRS values and recovery are different in a pig group ventilated with a mixture gas composed by argon compared with a group ventilated with common procedure; (3) to investigate the causes of the BRS variations in response to CA and following CPR. All the estimators adopted in this study show a significant decrease of the baroreflex after cardiac arrest (CA). However, a partial recovery is obtained in the last hours of post resuscitation. On one hand, this result could be explained by an increase of the vagal stimulation with a faster dynamics of baroreflex which drives the baroreflex gain recovery and, on the other, this recovery trend could be enhanced by a reduction of the cardiac electric instability, which however remains sustained in post-resuscitation. The same analyses applied on the two groups (argon and control) do not show significant differences in any considered indexes.

Abstract

Studi precedenti hanno dimostrato che il controllo della frequenza cardiaca da parte del riflesso barocettivo può essere impiegato per classificare la popolazione post-infarto e, in generale, quelle popolazioni affette da malattie cardiovascolari. L'attività barocettiva può essere valutata attraverso metodiche sia invasive, ossia per mezzo di farmaci, o non-invasive, ossia in condizioni spontanee. Questi metodi forniscono una stima dell'attività barocettiva misurata come *sensitività di baroriflesso* (BRS), che è espressa in $ms/mmhg$. Tuttavia, buona parte degli studi che utilizzano la BRS si concentrano sull'infarto miocardico (AMI) e non esistono studi di letteratura di significativa importanza, che investigano il ruolo della BRS durante e immediatamente dopo l'arresto cardiaco (CA). L'analisi degli effetti del CA sulla BRS potrebbe fornire un quadro più chiaro riguardo ai meccanismi coinvolti nella risposta del sistema cardiovascolare (CV) e quindi permettere di sviluppare un trattamento più efficace dei pazienti. Il presente lavoro si inserisce come prosecuzione del lavoro precedentemente pubblicato da Ristagno et al. (2014). In particolare, gli obiettivi di questa tesi sono: (1) studiare l'evoluzione della BRS dopo CA e nel successivo trattamento di CPR, come già fatto in maniera simile in precedenti studi, allo scopo di verificare se il recupero della stabilità cardiovascolare e della pressione arteriosa è accompagnata da un recupero dei valori di sensitività barocettiva in un modello animale di suino; (2) verificare se i valori di BRS e il loro recupero sono differenti in un gruppo di animali ventilati con una miscela di argon rispetto ad un gruppo con ventilazione meccanica con una miscela standard; (3) investigare le cause delle variazioni della BRS in risposta al CA e al successivo trattamento di rianimazione. Tutti gli stimatori della sensitività barocettiva mostrano un decremento significativo dopo l'arresto cardiaco. Tuttavia viene osservato un parziale recupero nel periodo successivo alla CPR. Da un lato, questo risultato può essere spiegato con l'aumento della stimolazione vagale mostrato anche da una dinamica più veloce del baroriflesso e che permette un parziale recupero della BRS, ma, dall'altro, questo

recupero parziale dei valori di BRS potrebbe essere anche favorito dalla riduzione dell'instabilità elettrica cardiaca, che rimane significativa anche dopo la rianimazione. Le stesse analisi applicate sui gruppi distintamente trattati con argon e controllo non hanno prodotto differenze significative in nessuno degli indici analizzati.

Acknowledgements

I would like to thank my "day-by-day" advisor, Prof.ssa Manuela Ferrario. Your advice, support, care and friendship are the reasons for the success of this thesis. Your leadership is truly inspiring. You have opened my eyes to the vast field of biomedical engineering, and I fully intend to pursue this field for the rest of my life.

Special thanks to my advisor, prof. Giuseppe Baselli, for his guidance and supervision throughout the research and writing process. Your constructive feedback and encouragement has been a great resource for this thesis.

I thank all my friends at Polimi. Dearest thanks to every member of the "big-family" for all those get-togethers and birthday showerings: I will treasure all those memorable moments. I would just mention Beatrice, Camilla, Claudio, Gian, Marta, Flo, Brunella, Franco and Rita.

I also thank all my friends at Bettolino. In particular, i cannot forget people like Luca, Federica, Maura, Antonio, Alessio, Ferri, the ASOCROMICHE party and Don Bruno. Their inspiration was pivotal to start my degree in Biomedical engineering.

Finally, I wish to thank my parents, my sister Isabel, my sister-in-law Elena, my brother Vito and the always special niece Arianna. Your support and believing in me helped me to complete this project and gain this result.

This work was possible thanks to experiments and research of prof. Giuseppe Ristagno.

Contents

Acknowledgements **1**

List of acronyms **9**

Executive summary **11**

Sommario **15**

1 Introduction **21**
1.1 Arterial blood pressure regulation: the autonomic nervous system 21
1.1.1 Baroreceptor reflex 24
1.1.2 The chemoreceptor reflex 26
1.1.3 An overview on the autonomic control 27
1.2 Baroreflex in impaired cardiovascular conditions 27
1.2.1 Acute myocardial infarction (AMI) 27
1.2.2 Occlusion of coronary artery (OCA) 30
1.2.3 Cardiac Arrest 31
1.2.4 Cardiac arrest and brain ischemic damage 32
1.3 Motivation 33
1.4 Thesis goals 34

2 Methods **35**
2.1 Database and experimental protocol description 35
2.2 The baroreflex estimation theory 38
2.2.1 The minimal model 38
2.2.2 Technical notes on porcine model 41
2.2.3 Non-parametric methods to estimate baroreflex gain . 42
2.2.4 Coherence 43
2.2.5 Bivariate model 45
2.2.6 Granger causality test 49

2.2.7 Impulse response analysis 50
2.2.8 Coefficient of sample Entropy 52
2.3 Data analysis 54
2.3.1 Data pre-processing and segment detection 54
2.3.2 Statistical analysis 56

3 Results **57**
3.1 Changes after CA 57
3.1.1 Cardiovascular changes in time-domain 57
3.1.2 Cardiovascular autonomic response in frequency domain 60
3.1.3 Granger causality test 66
3.1.4 Baroreflex indexes and coherence analysis 67
3.1.5 Impulse responses parameters 75
3.2 Comparisons between argon and control groups 78

4 Conclusions and future research **81**
4.1 Discussions 81
4.1.1 Autonomic response to cardiac arrest and baroreflex analysis 81
4.1.2 Comparison between Argon and control groups 83
4.2 Limitations and Further developments. 83
4.3 Conclusions 84

References **87**

List of Figures

1.1 ABP regulation mechanisms 23
1.2 The anatomic scheme of baroreflex 25
1.3 ANS blood pressure control 28
1.4 BRS dynamics after pPCI 30

2.1 Block diagram of autonomic interactions among RR, SAP and respiration 40
2.2 Block diagram of autonomic interactions, included cardiopulmonary reflex 41
2.3 Minimal model of autonomic interactions between RR and SAP 42
2.4 The *open-loop* $SAP \rightarrow RR$ transfer function 43
2.5 Examples of $G_{SAP \rightarrow RR}$ transfer function and $k^2_{SAP \rightarrow RR}$ coherence function 48
2.6 Example of $h_{ABR}(m)$ 52

3.1 The RR and SAP series and spectra 63
3.2 The DAP and PP series and spectra 64
3.3 The absolute RR power in the different experimental epochs . 65
3.4 The number of positive Granger tests for the feedback relation 66
3.5 The number of positive Granger tests for the feedforward relation 67
3.6 BRS in the different experimental epochs without thresholding the coherence 72
3.7 BRS in the different experimental epochs with surrogates method 73
3.8 $\beta_{RR \rightarrow SAP}$ in the different experimental epochs 74
3.9 Impulse response parameters in the different experimental epochs 77
3.10 BRS compared between argon and control group 80

List of Tables

2.1 The animals characteristics and outcomes of the two groups after CA and CPR 37

3.1 Time-domain moments of the first and second order in the different experimental epochs 59
3.2 Nonlinear indexes in the different experimental epochs 59
3.3 The spectral indexes in the different experimental epochs. . . 62
3.4 The number of the positive Granger tests in the different experimental epochs 68
3.5 The BRS values, computed with non-parametric and parametric methods, in the different experimental epochs 70
3.6 The difference of BRS values between Pre-CA and the other post-resuscitation phases 70
3.7 $k^2_{SAP\rightarrow RR}$ in the different experimental epochs 71
3.8 $\beta_{RR\rightarrow SAP}$ and $k^2_{RR\rightarrow SAP}$ values in the different experimental epochs 71
3.9 Impulse response parameters in the different experimental epochs 76
3.10 Comparison between argon and control group 79

List of acronyms

Symbols	Description
ECG	electrocardiogram
ABP	arterial blood pressure
CO	cardiac output
SV	stroke volume
RR	peek-to-peek interval on the ECG
SAP	sistolic arterial pressure
DAP	diastolic arterial pressure
PP	pulse pressure
ABR	arterial baroreflex response
BRS	baroreflex sensitivity
CA	cardiac arrest
OHCA	out-of-hospital cardiac arrest
Pre-CA	pre-cardiac arrest
Pr	post-resuscitation
LF	low frequency
HF	high frequency
CPR	cardiopulmonary resuscitation
CV	cardiovascular
COSEn	coefficient of sample entropy
LDS	local dynamic score
HRV	heart rate variability
PNS	parasympathetic nervous system
SNS	sympathetic nervous system
LAD	left anterior descending
OCA	occlusion of coronary artery
AMI	acute myocardial infarction

Executive Summary

Previous studies proved that the baroreceptor reflex (baroreflex) control of heart rate can be used for stratification of post-infarction population and, in general, cardiovascular diseases populations. The baroreflex can be assessed by different methods either invasive, by means of pharmacological manouver, or non-invasive, i.e. in spontaneous conditions. Those methods provide the baroreflex estimate known as baroreflex sensitivity (BRS) expressed as $ms/mmhg$ [1], [2], [3].

However, most of the studies that exploits BRS are focused on acute myocardial infarction (AMI) and there are no important literature works which investigate the role of BRS during and immediately after cardiac arrest (CA).

Grasner et al.[4] reported that the average incidence of the out-of-the-hospital CA (OHCA) is 38.7/100,000/year in Europe in a study that involved 37 communities as well as they found average OHCA incidence equal to 55/100,000/year in United States (considering the data represented in the study period 1980-2003). Furthermore, most of the CA patients that receive a successful CPR procedure die in the following 72 h for *post cardiac arrest syndrome*, that mainly includes ischemic brain damage [5].

Even though CA appeares to be one of the major threats to the cardiovascular physiology and it could profoundly influence the nervous system, BRS was not used as a predictive marker of post-CA population or as stratification index of outcomes. The analysis of the CA effects on the BRS could provide further knowledge about the mechanisms involved in the CV system response and thus paves the way for a more effective treatment.

The present work is a prosecution of the published work of Ristagno et al. [5]. In particular, the objectives of this thesis are (1) to study the

evolution of BRS after CA and following CPR as in previous studies [6] and to verify if the recovery of CV stability and arterial blood pressure is accompanied by a recovery of BRS values in porcine model; (2) to verify if the BRS values and recovery are different in a pig group ventilated with a mixture gas composed by argon compared with a group ventilated with common procedure; (3) to investigate the causes of the BRS variations in response to CA and following CPR.

As described by [5], the left anterior descending coronary artery was occluded in 12 pigs, and CA was induced. After 8 min of untreated CA, cardiopulmonary resuscitation was performed for 5 min before defibrillation. Following resuscitation, animals were subjected to 4 h ventilation with 70% argon-30% oxygen or 70% nitrogen-30% oxygen and ABP and ECG were measured during the experiment. In this research study RR, SAP, DAP and PP are extracted in the phase before CA (Pre-CA) and in post-resuscitation epochs after 1 h, 2 h, 3 h, 4 h. BRS is estimated in each experimental epochs with non-parametric methods and the bivariate model, described by [1], [2], [3]. In addition, time-domain and spectral indexes are computed as well as nonlinear indexes. Moreover, the *arterial baroreflex impulse response* (ABR) is estimated in each experimental epochs to further describe the baroreflex dynamics.

In time-domain, both RR and pressure variables averages present significantly changes during the experimental epochs. Furthermore, RR and PP do not recover after CA and their values are significantly lower with respect to the values measures before the event. In contrast, SAP and DAP increase with time course of the experiment, i.e. after resuscitation. The absolute RR power in LF band shows a decreasing trend after CA with a recovery in the following resuscitation period, even though the values are not significant. In contrast, the absolute PP power in LF band show a drop after CA without recovery. In similar way, LF components of SAP and DAP suggest a u shape in the observed time period (Table 3.3). Interestingly, RR total power diminishes after the onset of the impairing condition and recovers in the following post resuscitation epochs, as shown in Figure 3.3.

All the estimators adopted in this study show a significant decrease of the baroreflex after cardiac arrest (CA). However, a partial recovery is obtained in the last hours of post resuscitation. There are two possible explanations to this u shape evolution.

The first one is an electrical instability of the organ effector, which is the heart in the *closed loop system* that regulates ABP through CO. A second hypothesis is that the reduction of vagal stimulation and its recovery are the main drivers of the BRS variation. The recovery of PNS activity is underlined by the u shape trend of RR power in absolute units in HF band.

The impulse response analyses allows to investigate how the baroreflex changes not only in terms of gain but also in terms of temporal dynamics. The ABR delay reduces after CA and is significantly shorter at Pr 4h. This finding could be interpreted as a compensation mechanism to a BR gain reduction: a faster response but less large.

The partial recovery of baroreflex function could be thus seen by two perspectives: a recovery in dynamic gain (Table 3.5) and a reduction in time response, as shown by the impulse response analysis.

The same analyses applied on the two groups (argon and control) do not show significant differences in any considered indexes.

In conclusion, the present study investigates the BRS by means of different methods for each experimental different epoch after CA and these analyses confirm the presence of a partial recovery in the post resuscitation period. The argon has not any role to protect or preserve the baroreflex after CA or during PR and, in general, the autonomous nervous system functions. Finally, spectral and non linear analyses and impulse response investigation draw attention to some mechanism which develop after CA. On one hand, a recovery of the vagal stimulation with a faster dynamics of baroreflex drives the baroreflex recovery and, on the other, this trend towards a normal functioning could be enhanced by a reduction cardiac electric instability, which remains sustained in post-resuscitation.

Sommario

Studi precedenti hanno dimostrato che il controllo della frequenza cardiaca da parte del riflesso barocettivo può essere impiegato per classificare la popolazione post-infarto e, in generale, quelle popolazioni affette da malattie cardiovascolari. L'attività barocettiva può essere valutata attraverso metodiche sia invasive, ossia per mezzo di farmaci, o non-invasive, ossia in condizioni spontanee. Questi metodi forniscono una stima dell'attività barocettiva come *sensitività di baroriflesso* (BRS), che è espressa in $ms/mmhg$ [1], [2], [3].

Tuttavia, buona parte degli studi che utilizzano la BRS si concentrano sull'infarto miocardico (AMI) e non esistono studi di significativa importanza in letteratura, che investigano il ruolo della BRS durante e immediatamente dopo l'arresto cardiaco (CA).

Grasner et al. [4] hanno riportato che l'incidenza media dell'arresto cardiaco al di fuori dell'attività ospedaliera (OHCA) è pari a 38.7/100000/anno in Europa, in un studio che ha coinvolto 37 comunità. Inoltre, è stato calcolato che l'incidenza media di OCHA è pari a 55/100000/anno negli Stati Uniti (in uno studio che considera un periodo cha va dal 1980 al 2003). Inoltre, buona parte dei pazienti con CA a cui viene applicata con successo la *rianimazione cardiopolmonare* (CPR) muoiono nelle successive 72 h per la *sindrome da post-arresto cardiaco*, che induce principalmente ischemia cerebrale [5].

Sebbene l'arresto cardiaco sia chiaramente un evento con delle ripercussioni importanti sulla fisiologia cardiovascolare e il relativo controllo autonomico, fino ad ora non ci sono stati degli studi che si focalizzassero sul ruolo del baroriflesso sia come potenziale marker predittivo sia come indice per la stratificazioni di rischio in soggetti che hanno subito un arresto cardiaco post infarto. L'analisi degli effetti del CA sulla BRS potrebbe fornire un quadro

più chiaro riguardo ai meccanismi coinvolti nella risposta del sistema cardiovascolare (CV) e dare delle indicazioni per lo sviluppo di un trattamento più efficace dei pazienti.

Il presente lavoro si inserisce come prosecuzione del lavoro precedentmente pubblicato da Ristagno et al. [5]. In particolare, gli obiettivi di questa tesi sono: (1) studiare l'evoluzione della BRS dopo CA e nel successivo trattamento di CPR, come già fatto in maniera simile in precedenti studi allo scopo di verificare il recupero della stabilità cardiovascolare e della pressione arteriosa è accompagnata da un recupero dei valori di sensitività barocettiva in un modello animale di suino; (2) verificare se i valori di BRS e il loro recupero sono differenti in un gruppo di animali ventilati con una miscela di argon rispetto ad un gruppo con ventilazione meccanica con una miscela standard; (3) investigare le cause delle variazioni della BRS in risposta al CA e al successivo trattamento di rianimazione.

Come descritto in [5], il protocollo sperimentale consisteva nell'occlusione della coronaria discendente anteriore in 12 maiali per indurre l'arresto cardiaco. Dopo 8 minuti di arresto, la CPR è stata eseguita per 5 minuti dopo defibrillazione. A seguito della rianimazione, gli animali sono stati sottoposti a 4 ore di ventilazione meccanica con 70% argon - 30% ossigeno o 70% azoto - 30% ossigeno, a seconda del gruppo sperimentale assegnatogli. Pressione arteriosa (ABP) e ECG sono state misurate durante tutto l'esperimento. In questa studio, RR, SAP, DAP e PP sono estratte in ogni fase prima dell'arresto (pre-CA) e nei periodi dopo la rianimazione a 1 ora, 2, 3 e 4 ore dalla manovra di resuscitazione. La sensitività barocettiva è stimata in ogni epoca con metodi sia non-parametrici che basati sul modello bivariato, descritto da [1], [2], [3]. In aggiunta, sono stati calcolati indici sia nel dominio del tempo, sia spettrali, sia non-lineari. Infine, la risposta all'impulso del baroriflesso arterioso (ABR) è stimata in ogni epoca sperimentale per descrivere ulteriormente la dinamica barocettiva.

Nel dominio del tempo, i valori medi sia di RR che delle variabili pressorie presentano una variazione significativa nelle diverse epoche dell'esperimento. Inoltre, RR e PP non recuperano dopo l'arresto e i valori rimangono significativamente più bassi anche alla fine dell'esperimento rispetto ai valori prima di CA. Al contrario, i valori di SAP e DAP crescono durante il periodo successivo alla rianimazione. La potenza assoluta di RR nella banda LF decresce dopo CA e poi cresce, sebbene in maniera non significativa. Analogamente, anche le componenti LF di SAP e DAP mostrano un anda-

mento prima decrescente e poi crescente durante le epoche sperimentali Pr. Al contrario, la potenza assoluta della PP in LF non recupera. È interessante il fatto che la potenza totale della serie RR diminuisce dopo l'arresto e recupera nei tempi successivi alla rianimazione.

Tutti gli stimatori della sensitività barocettiva mostrano un decremento significativo dopo l'arresto cardiaco. Tuttavia viene osservato un parziale recupero nel periodo successivo alla CPR. Ci sono due possibili spiegazioni per questo trend.

Il primo è l'instabilità dell'organo effettore, cioè il cuore che secondo il modello ad anello chiuso regola la pressione tramite la regolazione del cardiac output. Questa instabilità è verificata attraverso misure non-lineare sulla serie RR. Una seconda spiegazione è la riduzione della stimolazione vagale. L'andamento della potenza assoluta della serie RR in banda HF, cioè la sua riduzione dopo il CA e il successivo incremento, sembrano associate alle variazioni dei valori di baroriflesso

L'analisi della risposta all'impulso ha permesso inoltre di investigare come il baroriflesso varia non solo in termini di guadagno, ma anche in termini di dinamica temporale. Il ritardo del picco della risposta del baroriflesso arterioso (ABR) si riduce dopo l'arresto ed è più corto a Pr 4h. Questo risultato può essere visto come un meccanismo di compensazione ad un ridotto guadagno di baroriflesso, cioè una risposta di minor entità ma più veloce.

Alla luce di questi risultati, il recupero delle funzioni del baroriflesso può essere visto da una doppia prospettiva: sia un recupero del guadagno dinamico di baroriflesso sia una riduzione dei tempi di risposta, come mostrato dall'analisi della risposta all'impulso. Le stesse analisi applicate sui gruppi distintamente trattati con argon e controllo non hanno prodotto differenze significative in nessuno degli indici analizzati, ma hanno confermato i trend ottenuti considerando tutti gli animali come un unico gruppo sperimentale.

In conclusione, la presente tesi ha analizzato il baroriflesso cardiaco con diverse metodologie e nelle diverse epoche sperimentali successive all'arresto cardiaco e i risultati ottenuti mostrano un parziale recupero del guadagno di baroriflesso accompagnato a un recupero della pressione arteriosa nelle ore seguenti la rianimazione cardiopolmonare. Infine, sia le analisi spettrali e non lineari che l'analisi della risposta all'impulso mettono in luce alcuni

meccanismi che si sviluppano e interagiscono dopo l'arresto cardiaco. Da un lato, il recupero della stimolazione vagale con una dinamica più veloce del baroriflesso permette un parziale recupero della BRS, ma, dall'altro, questo recupero parziale dei valori di guadagno di baroriflesso potrebbe essere favorito anche da una riduzione dell'instabilità elettrica cardiaca, che rimane significativa dopo la rianimazione. L'argon non ha alcun ruolo nel proteggere o preservare il baroriflesso dopo CA o durante la rianimazione e, in generale, non ha alcun ruolo nella protezione del sistema nervoso autonomo.

Chapter 1

Introduction

1.1 Arterial blood pressure regulation: the autonomic nervous system

The main role of the cardiovascular circulation is to support and fulfill the needs of body tissues, such as the transportation of nutrients, waste and oxygen as well as the communication of information through hormones or body defence through the diffusion of immune or inflammatory agents. In simple terms, the cardiovascular system is composed of a series of tubes (blood vessel) filled with fluid (blood) and connected to a pump (the heart). Pressure generated in the heart propels blood through the system continuously [7]. The blood flow rate from the cardiac pump called Cardiac Output (CO) is distributed to the various organs and tissues through the peripheral circulation, maintaining arterial blood pressure (ABP) in narrow range.

The amount of blood allocated to the different areas of the body, the pumping activity of the heart and the dynamics of the arterial pressure are regulated by the autonomous nervous system (ANS), which is part of the central nervous system (CNS). Its role is to control organs such as smooth muscles or the cardiac pump not under voluntary decisions. The two efferent branches of this system are the sympathetic nervous system (SNS) and the parasympathetic nervous system (PNS). The former one innervates most of the blood vessel, except for capillaries, and the heart. In the case of arterioles and small arteries, sympathetic stimulation could increase the resistance to the blood flow, mainly by the reduction of the diameter, leading to an increase of ABP and a deviation of blood to specific body areas. In the case of the veins, SNS could decrease their compliances, reducing the blood volume and pushing more blood into the heart. In the case of the

heart, the sympathetic stimulation increases the firing rate of the sino-atrial node and increases the muscle contractility of the myocardium [8], [7]. The PNS system innervates the heart though the vagus nerve, whose stimulation decreases the heart rate and the cardiac contractility [8], [7]. Nonetheless PNS actively influences only the heart activity, it could modify the level of ABP as a secondary effect due to the regulation of CO. On this perspective, the sympathetic and vagal stimulations act in combination in order to maintain blood pressure homeostasis.

The circulatory regulation is placed in the vasomotor centre, located in the reticular substance of the medulla and in the lower third of the pons [8]. It includes the nucleus of the solitary tract (NTS), the rostral ventrolateral medulla (RVLM), the caudal ventrolateral medulla (CVLM), dorsal motor nuclei (DMN) and nucleus ambiguous (NA). The ANS regulates the ABP, through a core network of neurons that also involve the hypothalamus and the spinal cord [9]. A very high level organization of this nervous controller is described as follows: RVLM is the main source of vessel vasoconstriction, projecting fibers to the spinal cord, in the pre-ganglionic neurons located in intermediolateral horn, and then to the vessels, passing through the sympathetic chain ganglia (located next to the vertebral column). The vagus nerve project to the heart from the DMN through NA, acting directly on the sino-atrial (SA) node. In contrast to the sympathetic branch, the PNS presents the preganglionic neuron located in the brain medulla and the postganglionic neuron next to organ it stimulates, e.g. the heart in the case of the vagus for the heart-rate regulation. The NTS receives sensory nerve signals through the glossopharyngeal nerve and the vagus and directly projects on the medullary area, thus providing *reflex control* of many circulator functions.

Aside from the exercise and stress functions, there are multiple subconscious control mechanisms that operate continuosly to maintain the arterial pressure at or near normal values and they are called negative reflex mechanisms [8]. These mechanisms provide an appropriate response to rapid changes in the cardiovascular system (CVS), in order to provide adequate blood flow to privileged regions (coronaries, kidneys and brain) and to redistribute it to specific regions according to respective metabolic demand. For these reasons they are known as short-term reflex mechanisms and they include the baroreflex, the cardiopulmonary reflex and the chemoreceptor mechanism. For sake of knowledge, it is important to say that ABP is also regulated by long-term mechanisms, which include the renal system by

means of the renin-angiotensin vasoconstriction and by the renal-blood volume pressure control as well as the stress relaxation of the vasculature and the capillary fluid shift. Alongside the short-term mechanisms, the CNS response to ischemia is an immediate ABP rise when the blood flow to the vasomotor centre is strongly reduced [8]. A summary of the ABP changes responses is reported in Figure 1.1. As the present thesis is focused on the cardiac baroreflex, the long-term mechanism are not discussed in this chapter.

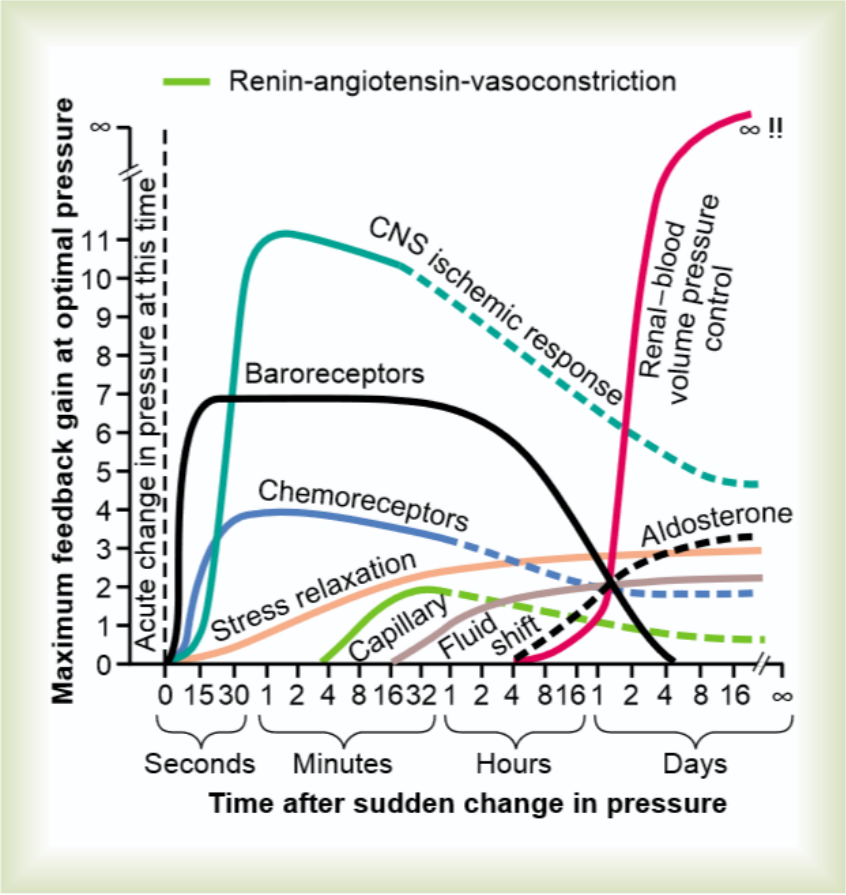

Figure 1.1: A synposis of long-term and short-term regulatory mechanisms of ABP regulation are reported from [8].

1.1.1 Baroreceptor reflex

The basic reflex to maintain ABP at homeostatic level is initiated by baroreceptors or pressoreceptors, which sense the stretch generated in vessels walls by ABP. This event let them transmit signals to the vasomotor centre through the NTS. The immediate consequence is an adjustment of ABP through the action of the heart by changing the cardiac output and of the blood circulation by modifying the resistance, in a feedback fashion. Baroreceptors are mechanosensitive nerve endings that respond to deformation or strain of the vessel walls in which they are located. Pressure is sensed by the baroreceptors in a multi-step process that includes pressure-mechanical deformation in the vessel wall followed by mechano-electrical transduction in the receptors themselves [10]. Mechanosensitive ion channels are present on baroreceptor nerve endings, and the influx of sodium and calcium through these channels is responsible for depolarization of baroreceptors during increased arterial pressure [11]. Baroreceptors in the aortic arch and carotid sinuses are known as high pressure baroreceptors, whereas cardiopulmonary baroreceptors in the atria, ventricles, vena cava, and pulmonary vasculature are often referred to as volume receptors or low pressure baroreceptors [12].

Arterial baroreceptors

As discussed above, the arterial baroreceptors are located in the aortic arch and carotid sinus: in particular, they can be found in the petrosal and nodose ganglia, respectively. A variation of ABP set point either a decrease or an increase provokes a modification in the tension of arterial wall, according to Laplace's Law

$$T = P * R \tag{1.1}$$

where P is the transmural pressure (N/m^2) and R is the the lumen radius, that induces a change in the arterial wall as shown by the following equation

$$\sigma = \frac{T}{h} \tag{1.2}$$

where h is the wall thickness. The modification in shear stress induced by ABP changes elicits variation in the baroreceptor afferent discharge. The signals from the baroreceptors in the carotid sinus are transmitted through the Hering's nerves to cranial nerve IX (glossopharyngeal) in the high neck, and then to NTS in the medullary area of the brain stem. Signal from

the mechanoreceptors in the aortic arch are transmitted through the cranial nerve X (vagus) to the same NTS. At this level, neurons project to the medullary vasomotor centre that mediates the sympathetic and parasympathetic outflows to the heart and the circulation. As discussed above, the sites that regulate the SNS stimulations are the CVLM and the RVLM, whereas the PNS discharge flows first through the dorsal motor nuclei and then through the nucleus ambiguous. The latter branch projects directly to the post-ganglionic using the vagus nerve, instead the former one projects to the spinal cord and then to the sympathetic chain, before reaching the efferent organs, such as arteries, veins and heart. Thus, if the NTS receive a signal due to an ABP increase, the vagal centers are excited while the sympathetic pathway is inhibited. The net effects are vasodilation of the veins and arterioles and decrease in heart rate and heart contractility. An ABP decrease switch the inhibition from the RVLM to the dorsal nuclei, leading to an increased heart rate and cardiac contraction force as well as the vasoconstriction of the various vessels. A scheme of baroreflex functioning is reported in Figure 1.2.

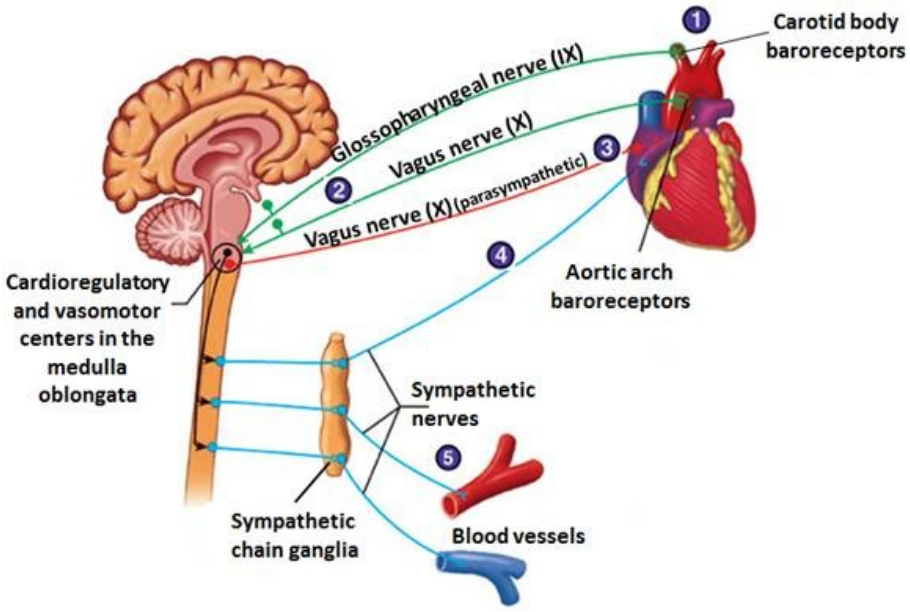

Figure 1.2: The anatomic scheme of baroreflex. In particular the afferents are highlighted in green, while the efferent are illustrated in red and blue.

Cardiopulmonary baroreceptors

Also called *low-pressure receptors*, they are located in cardiac atria, great veins and pulmonary vessels and they are similar to arterial baroreceptors because they sense mechanical stretch at vessel or atria walls. Their role is to minimize ABP changes in response to changes of blood volume, that is mostly contained by veins. The ANS response leads to an increase in HR and in total peripheral resistance if there is a reduction of venous return; in contrast, a decrease in HR and TPR is consequent of an increase in blood volume. What is actually sensed by pulmonary mechanoreceptors is central venous pressure (CVP) whose changes are elicited by volume shifts. HR changes in response to cardiopulmonary receptors have not the same extent as the changes induced by arterial baroreflex [13]. From an anatomical point of view, the afferent discharge of the receptor is projected to NTS through the cranial nerve X. The vasomotor centre is stimulated in case of sympathetic stimulation, leading to an increase of efferent discharge to vessels and the heart. On the opposite, in case of PNS stimulation, we have an inhibition of vasomotor centre, that actually induces a vasodilation for the absence of efferent discharge towards vessels as well as a direct vagal stimulation on the heart [8]. It is important to notice that direct effect on ventricular contractility by cardiopulmonary baroreceptors is not clarified yet. Furthermore, the Brainbridge reflex is matter of debate. It consists in an increase of HR in case of an increase of central blood volume, leading to a transient tachychardia in case high pressure in right atrium in contrast with the two types of baroreflex discussed above. The Bainbridge reflex has been proved in animals like dogs and rats, but not fully understood in humans, nonetheless some results hint a possible role in CV regulation in case of large variation of venous return [14].

1.1.2 The chemoreceptor reflex

Another mechanisms involved in ABP maintenance at homeostatic level is *respiratory control* initiated by chemoreceptors. They are located in chemoreceptors organs such as the *carotid bodies* and the *aortic arch* as well as a *chemosensitive area* locate in *respiratory center* of brain medulla. The latter is sensitive to change of partial pressure of arterial CO_2 (P_{aCO_2}) while the formers are sensitive to change of partial pressure of O_2 (P_{aO_2}) [8]. In contrast to baroreceptors, chemoreceptors respond to chemical stimuli, although they could control at the same time alveolar ventilation and arterial blood pressure. When central chemoreceptors detect an increase in P_{aCO_2} (hypercapnia) or peripheral chemoreceptors measure a decrease

in P_{aO_2} (hypoxia), the respiratory center induces an increase of the breath rate and depth of respiration. Furthermore, the respiratory center stimulates the vasomotor centre. The net effect is an increase of ABP thanks to vasoconstriction, although this reflex has a limited extent with respect to the cardiac baroreflex [8], [15]. From an anatomical point of view, the peripheral chemoreceptors transmits afferent signals through the vagus nerve to NTS, where the respiratory centre is located. The chemoreception process has been largely studied and reviewed for the peripheral [16], for the central [17], or both types [18] of receptors. In summary, chemoreflex closely interacts with the baroreflex [19] and it can be described as inhibitory effect [20].

1.1.3 An overview on the autonomic control

A summary of the all autonomic mechanisms which play a role in the short-term regulation of ABP are illustrated in Figure 1.3. As discussed above, the main controller is represented by the brainstem which actually influences the systemic arterial pressure in two ways:

1. The PNS and SNS afferents regulate the heart rate and heart contractility and they produce a change in cardiac output as net effect.

2. The sympathetic stimulation is able to act on vascular muscles to modify the TPR and thus acting on a local change on the ABP

The ABP is constantly monitored by the baroreceptors, but also by central *sensors* that monitor the brain perfusion. It can be also noticed that brainstem acts on respiratory movements through the chemoreceptors, represented by roman number IV in Figure 1.3, that can also act on TPR through the spinal cord. Furthemore, respiratory movements influence the venous return that can change ABP through CO.

1.2 Baroreflex in impaired cardiovascular conditions

1.2.1 Acute myocardial infarction (AMI)

Baroreflex sensitivity was investigated under different pathological or altered conditions. La Rovere et al. [22] found that BRS is a pivotal stratification marker in order to predict post-infarction outcomes. The ATRAMI

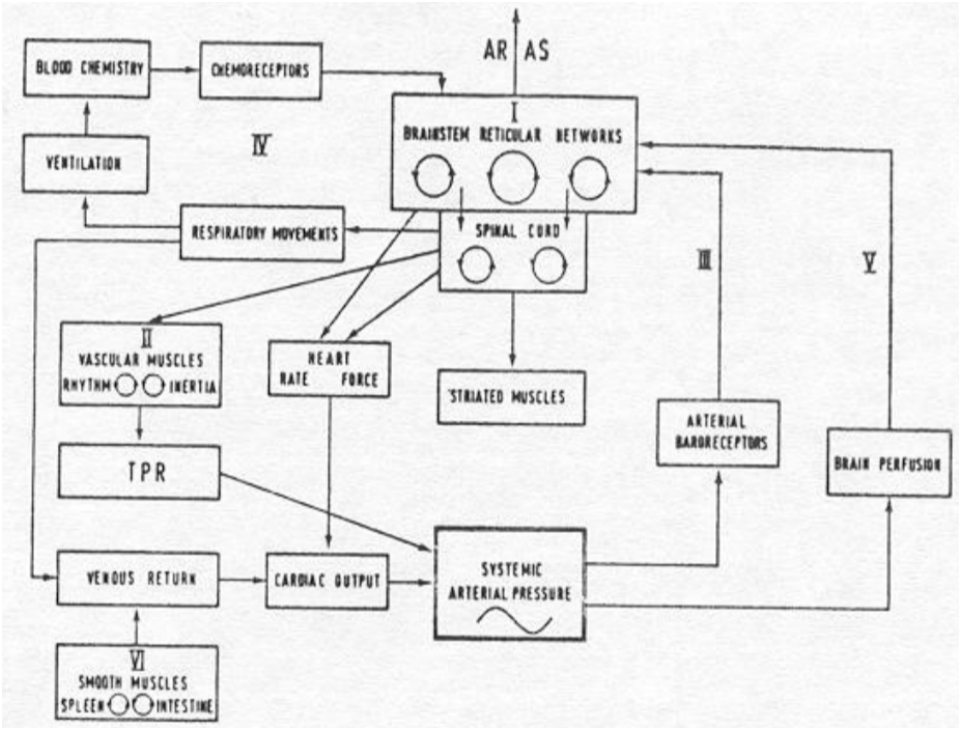

Figure 1.3: A summary of all short-term mechanisms of ANS blood pressure control, from [21].

(Autonomic Tone and Reflexes after Myocardial Infarction) study had the purpose to stratify the mortality risk in patients after a MI according to the values of several ANS measures [23], [24], [25], [26], like the standard deviation of all normal beats (SDNN). The study was motivated also by preceeding results suggesting a role of sympathetic hyperactivity in generating life-threatening arrhythmias, that could be antagonized by vagal activity [22], [27]. On this perspective, the ATRAMI study was designed to assess the prognostic values of BRS and SDNN for sudden cardiac death after AMI both as independent predictors or combined markers with other heart functionality measures, like the left ventricualr ejection fraction (LVEF). Even though BRS was evaluated using the invasive phenylephrine method [28], [29], patients with a BRS value below 3 $ms/mmhg$ and SDNN value below 70 ms have 1-year mortality extremely higher than patients with both well-preserved markers (15% vs 1%, $p < 0.0001$). These outcomes were confirmed even adding values of LVEF, that was reduced in association to the reduced values of BRS and ANS measures. This meant that ejection fraction could be low, but what determined cardiac mortality was actually the ANS control and its ability to properly regulate the cardiovascular system.

The authors concluded that the reduction in vagal activity is a key-point in the cardiac death and they suggested further experiments in order to verify improved outcomes in case of a modulation of the ANS to increase vagal tone and reduce sympathetic activity. From an engineering point of view, the ATRAMI study could be defined *static*, because it measured the BRS and SDNN 15 days after AMI. It did not look the evolution of the the ANS parameters by measuring them at different time intervals, e.g. starting from the hours immediately after the acute event.

The study of De Ferrari et al.[6] evaluated the baroreceptor reflex in patients after AMI with a longitudinal approach. In particular, they estimated the BRS among MI patients after primary percutaneous coronary intervention (pPCI) within the first 12h from intervention. In particular, they measured the baroreflex gain by means of the sequence method at 1h, 3h, 6h, 12h since the intervention was executed. The goals of the study were to evaluate the BRS in the acute phase of BRS, to investigate the clinical correlates of different BRS temporal patterns in the first hour after MI and to assess the influence of effective tissue reperfusion in modulating BRS. This study could be defined *dynamic* because it focused on the evolution of baroreceptor reflex in association to a longitudinal clinical assessment and outcome.

Patients with an effective tissue reperfusion had BRS values equal to 10.9 ± 6.4 $ms/mmhg$ one hour after the pPCI, but at the end of the follow-up BRS reached the following values 15.4 ± 5.2 $ms/mmhg$. A decrease around 70% of the ST-slope in ECG at 12h post-intervention was used as a reperfusion marker and it was called *ST-resolution*. Patient without the ST-resolution showed a decrease of the BRS values from 10.4 ± 6 $ms/mmhg$ to 8.4 ± 4.8 $ms/mmhg$ (Figure 1.4). Authors claimed to be the first to assess the BRS immediately after AMI reporting a dynamic pattern. Furthermore, they discussed conclusions similar to ones obtained by La Rovere [22]. Alongside the association between cardiac mortality and a reduced BRS gain, De Ferrari [6] hypothesized that baroreflex gain reduction was caused by an increase in afferents discharge associated to the left ventricle (LV) altered geometry, caused in turn by myocardial ischemia and necrosis. The consequence was an increase sympathetic activity and a decrease in vagal stimulation. The authors suggested the protective role of the vagus nerve from arrhythmias, highlighting also its ability to limit the inflammatory response and infarct size.

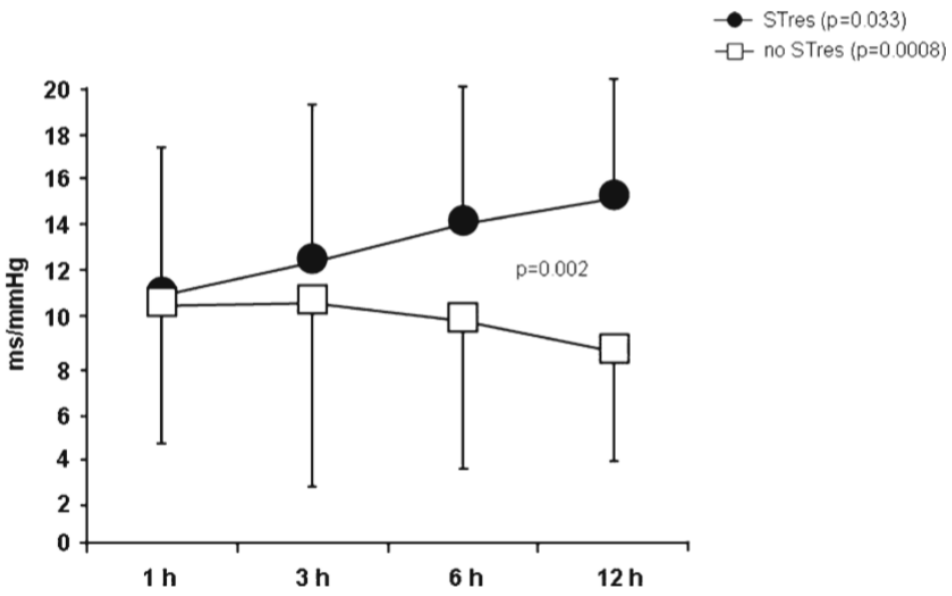

Figure 1.4: A comparison of BRS dynamic pattern after pPCI between the ST resolution group and the group without ST resolution, from [6].

1.2.2 Occlusion of coronary artery (OCA)

Another important pathological state under which BRS was studied is coronary occlusion. Airaksinen et el.[30] demonstrated that human baroreflex gain decreases immediately after OCA (30-60 s after the event).The estimation method was the phenylephrine method.This study was motivated by several evidences in animal models and by previous clinical studies like the La Rovere's one. This study had the purpose to verify if a low BRS can be considered as a marker of increased risk of ventricular fibrillation. In case of OCA, the experimental evidence clear confirmed that a reduced vagal tone and a sympathetic hyperactivity were associated to a decreased the baroreflex control of heart-rate and cause cardiac arrhythmias.

The results supported the hypothesis that the BRS decreases in response to an increase neural discharge of afferents. This hypothesis found further confirmation in the work of by Cerati et al. [31]. The authors measured the activity of the right branch of the cardiac vagus nerve immediately the electroneurogram (ENG) after OCA in 33 cats. The vagal activity increased

in the range between 39%-69% compared to the pre-occlusion level first minutes after the acute event occurred. This increase supposed to be a protective response to possible arrhythmias such as ventricular fibrillation (VF). However, after 10 minutes the vagal tone decreased below the pre-occlusion level and this reduction was more evident in cats that had a less increase in PNS activity after the OCA. These animals were also more susceptible to develop VF. Furthermore, a left stellectomy, i.e. a removal of the left stellate ganglion,which is the main source of afferent transmission for sympathetic stimulation, increases the vagal activity of 75% after OCA ($p < 0.01$) in comparisons with the same experimetal conditions without stellectomy.

The work of Babai et al.[32] presented results which further supports the hyphothesis so far illustrated in a canine model. In particular, the occlusion of left artery descendant artery (LAD) depressed the BRS. Further, the depressed vagal activity was found associated to this reduction and to a propensity to develop ventricular fibrillation (VF). The authors hypothesized the abnormal stretch of cardiac mechanoreceptors increase the SNS activity, exerting restraints on vagal activity. These results were supported also by experimental evidences reported in [33] and they are in agreement with the study of Cerati et al.[31]. The main finding of the study was a possible counter-measure to prevent BRS reduction. They verified that preconditioning of the LAD, that meant a previous occlusion of the artery for 5 mins 20 mins before the prolonged OCA of the experiment, was able to preserve BRS. This result was justified by the release of *myocardial protective substances*, such as bradykinins, prostanoids and nitric oxides, that modulate noradrenaline. The net effect was reduction of SNS activity and enhancement of the vagal stimulation, that had cardiac benefits discussed above.

1.2.3 Cardiac Arrest

To the best of our knowledge, there are no important literature works which investigate the role of BRS during and after cardiac arrest. Actually the CA was used as an end point of many studies, such as ATRAMI. The enrolled patients, whose BRS was investigated after myocardial infarction, were followed-up until they have cardiac arrest or sudden cardiac death. Cardiac arrest, also known as cardiopulmonary arrest or circulatory arrest, is a sudden stop in effective blood circulation due to the failure of the heart to contract effectively or not all. Common causes are arrhythmias such as VF. On this perspective, BRS was studied to predict the insurgence of CA after

AMI and its occurrence probability was found higher in ATRAMI patient [22]. Another interesting result was reported by Malik et al. [34]. They analyzed the ATRAMI database by including further indices, such as heart rate turbulence (HRT) as a surrogate of BRS to estimate the ANS influence on the post-infarction patients. The results showed that HRT as well as BRS and SDNN were able to predict the insurgence of fatal and non-fatal cardiac arrest. Furthemore, it confirmed that HRT is a useful surrogate to predict patients outcomes when BRS is not available.

However, reperfusion is known as the common procedure in case of CA and Bonnemeier et al.[35] investigated the HRT in patients that received percutaneous coronary intervention (PCI) and were classified according to recovery of the blood flow in arteries. It was found an improvement of HRT parameters, in particular of the turbulence slope (TS) improvement and the turbulence onset (TO), decreased [36] associated with patients with an effective reperfusion.

1.2.4 Cardiac arrest and brain ischemic damage

Ristagno and coworkers [5] recently investigated the *post-cardiac arrest syndrome* in a porcine model and this research study is an extension of this. Most of the patients undergo cardiopulmonary resuscitation (CPR) die in the first 72h due to the CA consequences: the main causes are the cardiac failure and the brain ischemic damage. The authors proposed the use of volatile anesthetics and noble gases, such as argon, in order to promote cerebral preservation. Even though they are inert, these gases are able to interact with amino acids of several enzymes and receptors, producing biological effects [37]. In particular, argon has shown neuroprotective properties [38], [37]. The authors hypothesized that argon would contrast postresuscitation neurological impairments. Twelve pigs underwent and were divided into argon-ventilated and control-ventilated group. The former one consisted of six pigs ventilated with a mixture of 70% argon and 30% oxygen during CPR. The latter six pigs were ventilated with 70% of nitrogen and 30% of oxygen. The argon group showed a significant better outcome in terms of neurologic recovery after CA. Similar results were reported in other animal models in literature [39]. The author suggested also that argon could be cardioprotective although the results were not statistical significant.

1.3 Motivation

Previous studies proved that the baroreceptor reflex (baroreflex) control of heart rate can be used for stratification of post-infarction population and, in general, cardiovascular diseases populations. The baroreflex can be assessed by different methods either invasive, by means of pharmacological manouver, or non-invasive, i.e. in spontaneous conditions. Those methods provide the baroreflex estimate known as baroreflex sensitivity (BRS) expressed as $ms/mmhg$ [1], [2], [3].

In addition, most of the studies that exploits baroreflex sensitivity (BRS) are focused on acute myocardial infarction (AMI) and there are no important literature works which investigate the role of BRS during and immediately after cardiac arrest.

According to American Heart Association, CA is caused by heart electrical system malfunctions such as ventricular fibrillation, or it can be consequent to myocardial ischemia due to coronary occlusion. In case of severe arrhythmias, cardiac impulses go berserk inducing contraction of some areas of ventricular muscles and relaxation of other areas at the same time. This state leads to a persistent partial contraction of the heart that is definitely insufficient to pump blood in pulmonary and systemic circulation. In case of cardiac ischemia, a low blood perfusion cause a dramatic loss of cardiac contractility and a severe arrhythmias can occur as well before CA. Common counter-measures to reverse this life-threatening event are the cardiopulmonary resuscitation (CPR) in order to restore reperfusion and defibrillation to restore the normal heart rhythm. AMI could cause CA or sudden cardiac death, in particular after acute coronary occlusion. Grasner et al.[4] reported that the average incidence of the out-of-the-hospital CA (OHCA) is 38.7/100,000/year in Europe in a study that involved 37 communities as well as they found average OHCA incidence equal to 55/100,000/year in United States (considering the data represented in the study period 1980-2003). Furthermore, most of the CA patients that receive a successful CPR procedure die in the following 72 h for *post cardiac arrest syndrome*, that mainly includes ischemic brain damage [5].

Even though CA appeared to be one of the major threats to the cardiovascular physiology and it could profoundly influence the nervous system, BRS was not used as a predictive marker of post-CA population or as stratification index of outcomes. Although baroreflex is the direct expression

of nervous regulation of the heart rate and arterial blood pressure (ABP) and it can provide an overall assessment of the ANS and the cardiovascular system at the same time, there are not studies which focus on the evolution of BRS values after CA. The analysis of the CA effects on the BRS could provide further knowledge about the mechanism involved in the CV system response and thus paves the way for a more effective treatment.

1.4 Thesis goals

The present work is a prosecution of the published work of Ristagno et al. [5]. The experimental setup and animal data are the same (a detailed description is provided in the next chapter). In particular, the objectives of this thesis are:

1. To study the evolution of BRS after CA and following CPR as in other studies [6] and to verify if the recovery of CV stability and arterial blood pressure is accompanied by a recovery of BRS values. The baroreflex gain estimation is performed with different methods and without pharmacological manouvers. In addition, an impulse response analysis is performed as well in order to investigate the dynamic response and not only the absolute gain of the baroreflex, by adopting apporaches from System Identification engineering.

2. To verify if the BRS values and recovery are different in the two pigs groups according to the different treatment.

3. To investigate the causes of the BRS variations in response to CA and following CPR.

Chapter 2

Methods

2.1 Database and experimental protocol description

This work is the prosecution of a previous study [5]. The description of the animal preparation and experimental protocols is detailed in the follow. Twelve male pigs ($38 \pm 1\ kg$) received anesthesia by intramuscular injection of ketamine ($20\ mg/kg$) and completed by ear vein injection of sodium pentobarbital ($30\ mg/kg$). Additional doses of pentobarbital ($8\ mg/kg$) were administered at intervals of approximately $1\ h$. A cuffed tracheal tube was placed, and animals were mechanically ventilated with a tidal volume of 15 mL/kg and F_{IO_2} of 0.21. Respiratory frequency was adjusted to maintain the end-tidal P_{CO_2} (ET_{CO_2}) between 35 and 40 $mmHg$, monitored with an infrared capnometer [40] [41]. A fluid-filled 7F catheter was advanced from the right femoral artery into the thoracic aorta and used for the continuous recording of central ABP.

Myocardial infarction was induced in a closed-chest preparation by intraluminal occlusion of the left anterior descending (LAD) coronary artery with the aid of a 6F balloon-tipped catheter inserted from the right common carotid artery [40]. For inducing ventricular fibrillation (VF), a 5F pacing catheter was advanced from the right subclavian vein into the right ventricle [41]. The position of all catheters was confirmed by characteristic pressure morphology and/or fluoroscopy. ECG electrodes were placed in the frontal plane and continuously recorded during the experiment. The animals were allocated into one of the two study groups: (a) *argon treatment*, the animal were ventilated during the resuscitation with a gas mixture composed by 70% argon and 30% oxygen; or (b) *control treatment*, during the resus-

citation a standard gas mixture was used, i.e a mix of 70% nitrogen and 30% oxygen. Argon or control treatment was initiated within 5 min following resuscitation, after hemodynamic stabilization. The balloon of the LAD coronary artery catheter was inflated with 0.7 mL of air to occlude the flow. If VF did not occur spontaneously, after 10 min it was induced with 1 to 2 mA AC current delivered to the right ventricle endocardium. Ventilation was discontinued after onset of VF. After 8 min of untreated VF, CPR, including chest compressions with the LUCAS 2 (PhysioControl Inc, Lund, Sweden) and ventilation with oxygen was initiated. After 5 min of CPR, defibrillation was attempted with a single biphasic 150-J shock, using an MRx defibrillator (Philips Medical Systems, Andover, MA). If resuscitation was not achieved, CPR was resumed and continued for 1 min before a subsequent defibrillation. Adrenaline (30 $\mu g/kg$) was administered via the right atrium after 2 and 7 min of CPR.

Successful resuscitation was defined as restoration of an organized cardiac rhythm with a mean arterial pressure (MAP) higher than 60 $mmHg$, which persisted for more than 1 min. After that, if VF reoccurred, it was treated by immediate defibrillation. After successful resuscitation, anesthesia was maintained, and animals were monitored for the following 4 hours. Forty-five minutes after resuscitation, the LAD coronary artery catheter was withdrawn. Temperature of the animals was maintained at 38 °C ± 0.5 °C during the whole experiment. After 4 h of treatment, catheters were removed, wounds were repaired, and the animals were extubated and returned to their cages. Analgesia with butorphanol (0.1 mg/kg) was administered by intramuscular injection. At the end of the 72-h postresuscitation observation, animals were reanesthetized for echocardiographic examination and blood sample withdrawn. Animals were then killed painlessly with an intravenous injection of 150 mg/kg pentobarbital. Hemodynamics, ET_{CO_2} and electrocardiogram were recorded continuously (WinDaq DATAQ Instruments Inc, Akron, OH).

The summary of the experimental groups and their groups and their characteristics are reported in Table 2.1.

Experiment outcomes	Argon	Control
Time from OCA to VF (min)	9±1	9±2
Coronary perfusion pressure ($mmHg$)		
CPR 1 min	25±4	33±5
CPR 3 min	47±11	44±4
CPR 5 min	42±7	35±3
Duration of CPR before resuscitation (s)	337±24	353±42
Total dose of adrenaline administered (mg)	1.3±0.2	1.5±0.3
Total defibrillations delivered	12±6	6±2
Successful resuscitation	6/6	6/6
72 h Survival	6/6	5/6
Right atrial pressure ($mmhg$)		
Pre CA	4±1	5±1
Pr 2 h	5±1	7±1
Pr 4 h	5±1	6±1
ET_{CO_2} ($mmhg$)		
Pre-CA	36±1	35± 0
Pr 2 h	36±0	36± 0
Pr 4 h	38±1	36± 1
LV cardiac output (L/min)		
Pre-CA	4.5±0.3	4.2±0.6
Pr 2 h	3.6±0.6	3.3±0.4
Pr 4 h	3.9±0.5	3.3±0.3
LV EF (%)		
Pre CA	69±2	69±2
Pr 2 h	39±2	35±6
Pr 4 h	48±7	46±5
Pr 72 h	67±5	61±2
Total sodium pentobarbital administered (mg)	1606±95	1613±120

Table 2.1: Data of the experimental groups and their characteristics. CPR= cardiopulmonary resuscitation; Pre-CA= pre-cardiac arrest; Pr=post resuscitation; ETCO2=end tidal pressure CO_2; LVEF=left ventricular ejection fraction, from [5].

2.2 The baroreflex estimation theory

2.2.1 The minimal model

Since its discovery as clinical tool, the BRS was used to be estimated with phelynephrine method or similar techniques for a long time [28], [29]. Even though it is recognized as simple and easy-to-understand method, this approach has many drawbacks:

- It is invasive. Although current technologies for beat-to-beat mesurement ABP does not require direct access to vessels, phenylephrine is a vasoconstrictor drug that causes an increase in the blood pressure and can cause a decrease in heart rate through reflex bradycardia. This procedure could not be feasible in patients as it can compromise an already unstable conditions.

- Phenylephrine interacts with the ANS. It works as adrenergic receptors agonist, showing properties similar to adrenaline. This means that it works as sympathetic stimulation. Even though the vasoconstriction is meant to induce the vagal reaction on the heart in order to measure the BRS, this could interact in unknown manners in people with cardiovascular diseases, such as hypertension.

- Furthermore, this method was introduced in order to have an estimation of BRS by *opening the control loop*. It means that phenylephrine vasoconstriction replaces the ANS control on vessels and limits any heart rate changes in response to the externally induced ABP increase. This approach is helpful to study the feedback mechanism of baroreceptors to induce heart rate changes according to ABP level, because, for few seconds, there are no ways to adjust ABP increase imposed by the external cause, i.e the drug. On this perspective, the cardiovascular system is seen as I/O system where the input is ABP and the output is HR. However, this modeling is far from reality in which HR and ABP interact each other. Indeed, the ANS aims to regulate the ABP through the HR, when ABP changes are detected. The physiological system works actually in *closed loop*. Although phenylephrine was the first useful method to estimate the baroreflex gain, it works by *opening the loop* and modifies the physiological, limiting any possible vasodilation to contrast the ABP increase. Furthermore, the heart rate is decreased, but ABP is not set to normal levels until the phenylephrine is still active, as discussed above. In summary, BRS is

measured when the system is disturbed, that is not the normal condition in which baroreflex is used to acting. In particular, this approach could also bias the BRS estimation in individuals with pathologies, where the ANS is already altered.

According to what is discussed in Chapter 1, the main physiological variables involved in ABP short-term regulation are arterial blood pressure itself, the heart rate, the central venous pressure and the tidal volume, whose interrelationships are regulated through the SNS and the PNS activities, determining what is called autonomous variability [42]. A summary of these connections is reported in Figure 1.3. The oscillations of heart rate on average value are called *heart rate variability* (HRV) as well as the *blood pressure variability* stands for the continuous changes of systolic and diastolic blood pressure. This phenomenon was known as "Mayer waves" for a long time. In particular, these cyclic changes of the RR interval, so called from the distance between two consecutive R peaks in an ECG recording, and the systolic arterial pressure (SAP) are quantified through power spectral analysis [43]. The spectral LF power component (0.04-0.15 Hz) represents the sympathetic activity on the heart and the vessels. In contrast, the HF power component (0.15-0.4 Hz) represents the vagal activity and respiratory effects on the heart.

However, this represents a univariate method to quantify the autonomic activity on cardiovascular signals [42]. One way of overcoming the limitations analysis is to consider the relationships between pairs of variables [42]. For instance we should necessarily take in account not only the baroreflex for ABP regulation, but also *the mechanical feedforward*. In fact, changes in RR intervals induces changes in SAP through cardiac output. This is consequence of Frank-Starling and Windkessel run-off effects [2].

Another important factor that influences HR and ABP is respiration. Respiration has mechanical effect on blood pressure, indeed lung inflation induces intrathoracic pressure decrease that shifts blood in cardiopulmonary compartment and reduces ABP [44], [45]. This effect is usually referred to as *respiratory sinus arrhythmia* (RSA), a term that summarizes all the mechanisms that have an overall effect on heart rate through respiration. The most important one is the direct coupling between respiratory center in the medulla and the autonomic centre that influences the heart rate. The second one is the vagal feedback mediated by pulmonary stretch receptors [44]. The latter heart-rate mechanisms actually form the *respiratory cardiac cou-*

pling, that combines with the baroreflex response respiratory-related ABP fluctuations in RSA [42].

The physiological interactions between RR, SAP and the respiratory signal, that represents instantaneous lung volume inspired every heart beat, are summarized in system dynamics terms by the blocks diagram in Figure 2.1.

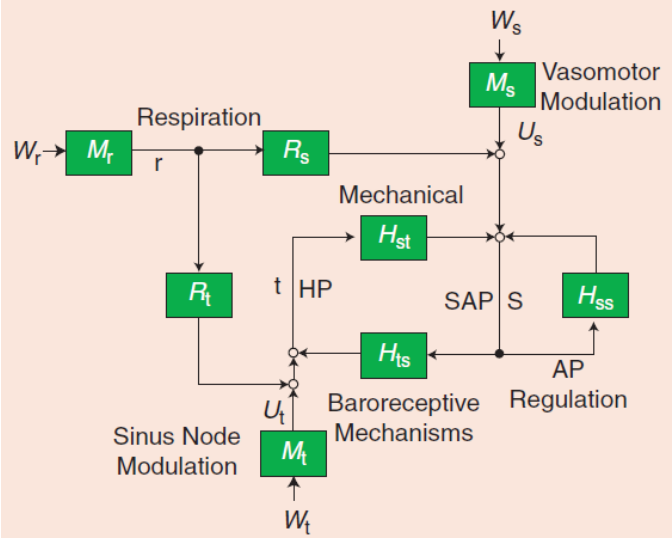

Figure 2.1: A block diagram of all autonomic interactions among RR, SAP and respiratory signal. H_{st} represents the baroreflex block. See for more details [1], [2], [46].

The baroreflex is represented by the *transfer function* H_{ts} with SAP as input and RR as output. On the opposite, the *transfer function* H_{st} stands for the mechanical feedforward through CO mediated changes, with RR as input and SAP as output. The two blocks form together a *closed loop*. The scheme also reports:

- The block M_s that summarizes all the external influence on the SAP variable
- The block M_t that summarizes all the external influence on the RR variable
- Blocks R_t and R_s represent the external influence of respiration variable on the cardiovascular variables RR and SAP. The two *transfer functions* represent respectively the RSA and the mechanical effect of respiration on SAP.

- The block M_r that summarize all the external influence on the respiration variable
- The block H_{ss} represent the ABP auto-regulation.

Even though this model is the complete system for short-term ABP regulation, the research presented in this thesis does not have the possibility to consider the complete model, for the simple reason that the respiratory signal is not available. Furthemore, the complexity of the model in Figure 2.1 can be increased taking in account the cardiopulmonary effect as reported in Figure 2.2. The model considered in this work is reported in Figure 2.3, in which only the RR signal and the SAP are taken into account. This modeling approach is considered "minimal model" [42] in contrast with a structured and large scale model that tries to include all the possible ABP regulation mechanisms explained by differential equations [47]. If the last approach could deepen the physiological view of the pressure homeostasis, the former is able to take account most of the ABP dynamics with a strongly reduced number of parameters to be estimated.

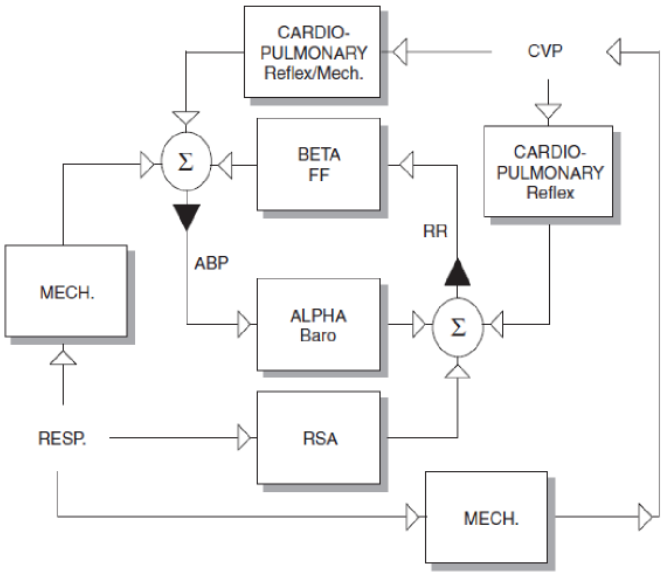

Figure 2.2: A more complete diagram in which the cardiopulmonary reflex is also included. Figure from [48], [3].

2.2.2 Technical notes on porcine model

The reported models are described for human physiology. According to VonBorrel [49] and Horner [50], the frequency bands commonly used for the

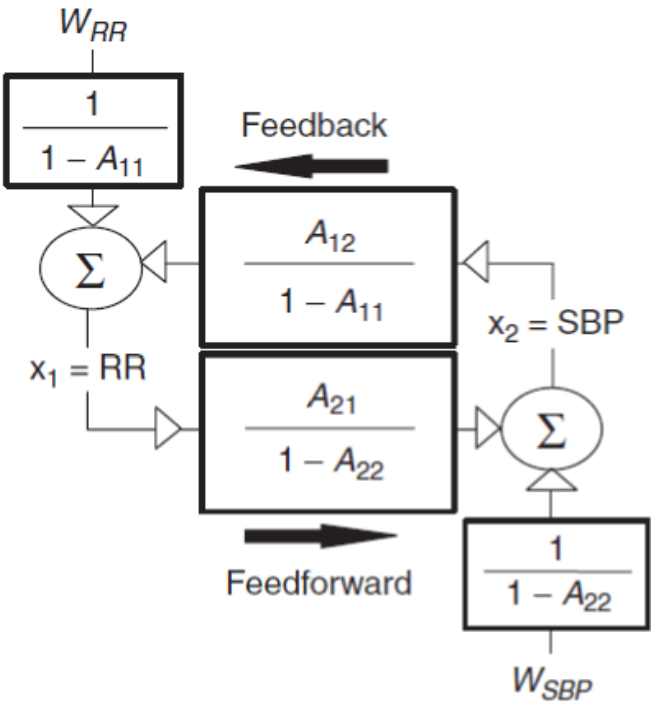

Figure 2.3: A simplified diagram of short-term ABP regulation from [48]. The only variables reported are RR and SAP, labelled as SBP in the panel.

CV signals such as HRV, are similar to humans. Furthermore, the porcine model is frequently used to test cardiovascular surgery due to the strong similarity with the man. Hence, the model in Figure 2.3 is supposed to hold also for the pigs. Another methodological consideration regards the recorded signals. Although the described scheme speaks about RR interval, the used variable is the *heart period* (HP), that represents the interval between two consequent ABP onsets. See §2.3.1 for further details.

2.2.3 Non-parametric methods to estimate baroreflex gain

BRS indices are estimated by two non-parametric methods: the spectral method and the transfer function method. The first one requires the SAP and RR spectra and the BRS index is estimated as the ratio in LF an HF band separately

$$\alpha_{LF} = \sqrt{\frac{S_{RR}(LF)}{S_{SAP}(LF)}} \tag{2.1}$$

$$\alpha_{HF} = \sqrt{\frac{S_{RR}(HF)}{S_{SAP}(HF)}} \tag{2.2}$$

The second one estimates the BRS as the average gain of the transfer function from SAP to RR in LF and HF bands with

$$H_{RR,SAP}(f) = \frac{S_{cross}(f)}{S_{SAP}(f)} \tag{2.3}$$

where S_{SAP} is SAP spectrum and S_{cross} is the cross-spectrum between SAP and RR time series. The cross-spectrum is estimated by applying a moving average Parzen windowing. The time series is subdivided in sequence of 1/4 original length and overlapped by 50%. Actually the method is called non-parametric because the relation between SAP and RR do not underline a specific model, but it considers a correlation between the two signals estimated in the frequency domain. The method is still called non-parametric although the spectra of the signals could be estimated through an autoregressive model. The reported approaches can be described by the simple diagram in Figure 2.4, where only SAP taken into account as influencing factor of RR intervals in *open-loop* fashion. Although these mathematical approaches do not require invasive manoeuvres, they do not take into account other mechanisms that are actually present in human physiology. The scheme is actually true if and only if RR changes are not able to markly influence SAP values, respecting the *casuality* hypothesis. On physiological perspective, this is only true when the *mechanical feedforward* is limited, that is actually possible with an external cause, such as phenylephrine. However, due to their simplicity, these methods find a large application in physiological research.

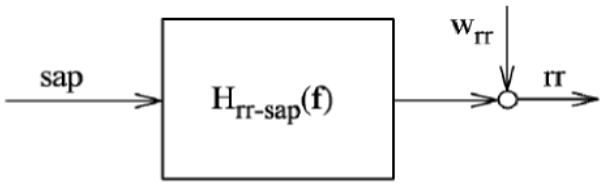

Figure 2.4: The transfer function method is based on the existance of the reported open-loop *relationship. This figure was retrieved by [1].*

2.2.4 Coherence

The coherence function estimates the degree of coupling between two signals in the frequency domain. The coherence is derived by calculating the magnitude of the cross-spectral density function between the two series and

normalized by the auto-spectral density functions. The coherence function assumes values between zero (absence of correlation) and one (complete correlation). The coherence between SAP and RR is estimated by

$$K^2_{RR,SAP}(f) = \frac{|S_{cross}(f)|^2}{S_{SAP}(f) * S_{RR}(f)} \tag{2.4}$$

High coherence between two signals is commonly defined when the magnitude expressed by (2.4) is greater than 0.5 [51], [45], [52], [53], [54]. This threshold is applied separately in the LF and HF bands in order to find the frequencies whose corresponding values of *transfer function* (TF) are then averaged. The coherence function is important not only for the estimation of the BRS with the TF but also for the bivariate model, as discussed below. Pathological conditions may affect dramatically the power in each individual signal such as heart rate variability and SAP variability, thus producing a very low coherence values. In this cases the choice of a threshold could be critical [55], [22], [56], [57]. Moreover, it was recently shown that the error of gain function estimates depends more on other parameters than the coherence estimation itself [57]. These observations suggest that the choice of an arbitrary fixed threshold equal to 0.5 is questionable [58]. In the present work, two possible criteria to estimate the BRS from the gain function are proposed:

- The first one includes the average of all points in the considered frequency band regardless the coherence value. According to Pinna et al. [59], in conditions of low signal-to-noise ratio and/or impaired baroreflex gain with a markedly reduced coherence, the simple average of the gain function in the LF band allows a sufficiently accurate BRS estimation.

- A "tailored" threshold for each frequency according to surrogates method reported in [58].

The second criteria investigates the threshold by applying a statistical approach on the sampling distribution of the coherence estimator. The coherence computation can be seen as an estimator $\hat{k}^2_{RR,SAP}$, which is thus affected by errors and could assume nonzero values even though $k^2_{RR,SAP}$ is equal to zero. A threshold in the coherence has to be defined for determining whether two series SAP and RR are significantly coupled in our case. In agreement with hypothesis testing [60], the sampling distribution derived in case of absence of coupled is used to test the null hypothesis of coherence equal to zero according to a predefined significance level (usually $\alpha = 0.05$).

With this statistical definition, a coherence greater than the threshold leads to reject the null hypothesis and supports the presence of significant coupling. The coherence distribution in absence of coupling is obtained through surrogates [61], [62].

An ensemble of N pairs of surrogate time series are generated by imposing the same linear features of the original time series, i.e. values distribution and spectral densities, but shuffling the values. In this research study, N is put equal to 100. The detailed description of the surrogate methods can be found in [62], [83], [84]. The coherence was then estimated between each pair of surrogate series and thus a probability distribution of coherence values is available for each frequency. The threshold $T(f)$ to test the null hypothesis is then set at the percentile $100(1-\alpha)$ of the coherence sampling distribution, with $\alpha = 0.05$ as the significance level of the statistical test [60].

2.2.5 Bivariate model

The bivariate closed loop model assesses the casual relationship from RR to SAP, i.e. the *mechanical feedforward*, and from SAP to RR, i.e. the *feedback* mechanism, the actual cardiac baroreflex [48]. As already observed, the system is *bivariate* because RR and SAP are the only two considered signals: the respiration signal is not available. The reference scheme is reported in Figure 2.3. The relationship $SAP \rightarrow RR$ stands for the arterial baroreceptor reflex, whereas the relationship $RR \rightarrow SAP$ represents the direct influence of RR interval on SAP, which is not mediated by autonomic control and consists in a perturbation mechanism based on the Starling law, i.e an increased stroke volume (SV) with a longer RR, and on the diastolic runoff. The last one represents a larger decay of DAP with a longer RR that decreases SAP and keeps constant other variables like SV [48], [63], [64]. The autoregressive bivariate model can be expressed by the following matrix form:

$$\mathbf{X}(n) = \sum_{k=1}^{p} \mathbf{A}(k) * \mathbf{X}(n-k) + \mathbf{W}(n) \tag{2.5}$$

where

$$\mathbf{A}(k) = \begin{bmatrix} a_{11}(k) & a_{12}(k) \\ a_{21}(k) & a_{22}(k) \end{bmatrix}$$

$$\mathbf{X}(n) = \begin{bmatrix} RR(n) \\ \mathrm{SAP}(n) \end{bmatrix}$$

$$\mathbf{W}(n) = \begin{bmatrix} w_{RR}(n) \\ w_{SAP}(n) \end{bmatrix}$$

and the coefficients a_{ij} are then used to calculate the gains of the transfer functions:

$$G_{SAP \to RR}(f) = \frac{A_{12}(f)}{1 - A_{11}(f)} \tag{2.6}$$

$$G_{RR \to SAP}(f) = \frac{A_{21}(f)}{1 - A_{22}(f)} \tag{2.7}$$

where $A_{ij}(f) = \sum_{k=1}^{p} a_{ij} e^{-j2\pi fk}$. $\mathbf{A}(k)$ matrices and the variances of the input noises $w_i(n)$ are estimated through the Yule-Walker equations through an extended version of the Levinson-Wiggins-Robinson algorithm [65]. The order p of the model was set equal to 8.
The transfer functions $G_{SAP \to RR}$ and $G_{RR \to SAP}$ represents respectively the blocks H_{ts} and H_{st} in Figure 2.1. Furthermore, the expressions in (2.6) and (2.7) are the same reported in Figure 2.3. The values of the gains $G_{SAP \to RR}$ and $G_{RR \to SAP}$ associated to LF and HF band were calculated, according to the procedure reported in [48], [63]. In particular,

- They are computed as the average of all values of the function $G(f)$ at each frequency regardless the coherence
- They are computed as the average of values of the function $G(f)$ at the frequencies which correspond a coherence value higher than the computed threshold, as described before.

Given the AR bivariate process described by (2.5), auto- and cross-spectra are obtained as diagonal and non-diagonal elements of

$$\mathbf{S}(f) = \mathbf{H}(z) \cdot \Sigma \cdot \mathbf{H'}(z^{-1}) \tag{2.8}$$

where $\mathbf{H}(z) = (\mathbf{I} - \mathbf{A}(z))^{-1}$, $\mathbf{H'}(z^{-1})$is the transpose matrix of $\mathbf{H}(z^{-1})$, Σ is the variance matrix of $\mathbf{W}(n)$. The power spectra of y_1 (RR) and y_2 (SAP) are respectively

$$S_{11}(f) = |\Delta(z)|^2 \cdot [|1 - A_{22}(z)|^2 \cdot \lambda_1^2 + |A_{12}(z)|^2 \cdot \lambda_2^2]|_{z=e^{j2\pi f \Delta t}} \tag{2.9}$$

and

$$S_{22}(f) = |\Delta(z)|^2 \cdot [|A_{21}(z)|^2 \cdot \lambda_1^2 + |1 - A_{11}(z)|^2 \cdot \lambda_2^2]|_{z=e^{j2\pi f \Delta t}} \tag{2.10}$$

while the cross-spectrum is

$$\begin{aligned} S_{12}(f) =& |\Delta(z)|^2 \cdot [(1 - A_{22}(z))(A_{21}(z^{-1})) \cdot \lambda_1^2 + \\ & (A_{12}(z)) \cdot (1 - A_{11}(z^{-1})) \cdot \lambda_2^2]|_{z=e^{j2\pi f \Delta t}} \end{aligned} \tag{2.11}$$

with $\Delta(z) = ((1 - A_{11}(z)) \cdot (1 - A_{22}(z)) - A_{12}(z) \cdot A_{21}(z))^{-1}$. Equations (2.9) and (2.10) show that the power spectrum of y_i is the sum of two parts, depending on the influences of y_i on y_i through $A_{ii}(z)$ and on the causal effect of y_j on y_i through $A_{ij}(z)$, respectively. Equation (2.11) shows that the cross-spectrum is also the sum of two parts, but both the components depend on causal relationships between y_1 and y_2: the first term depends entirely on $y_1 \rightarrow y_2$ causality through $A_{21}(z)$, while the second one depends on $y_2 \rightarrow y_1$ causality through $A_{12}(z)$. If the coherence $k^2_{RR,SAP}$ is rewritten as

$$k^2_{12}(f) = \frac{|S_{12}(f)|^2}{S_{11}(f) * S_{22}(f)} \tag{2.12}$$

The two causal coherence functions can be estimated as

$$k^2_{1\rightarrow 2}(f) = k^2_{12}(f)|_{A_{12}(z)=0} \tag{2.13}$$

$$k^2_{2\rightarrow 1}(f) = k^2_{12}(f)|_{A_{21}(z)=0} \tag{2.14}$$

which quantify the strength of the linear relationship in the $y_1 \rightarrow y_2$ (*feed-forward*) and $y_2 \rightarrow y_1$ (*feedback*). In this study, the average of the causal coherence is computed in LF and HF band by considering the adapting threshold and the surrogates estimation and also by considering the entire frequency band.

An example of baroreflex transfer function is reported in Figure 2.5, computed with (2.6). Examples of causal coherence and coherence threshold defined with the surrogates method are reported in Figure 2.5: the blue graph stands for a *feedback* casual coherence ($k^2_{SAP\rightarrow RR}$), while the red line is the threshold in function of frequency, whose computation is according to Faes [58], as described above.

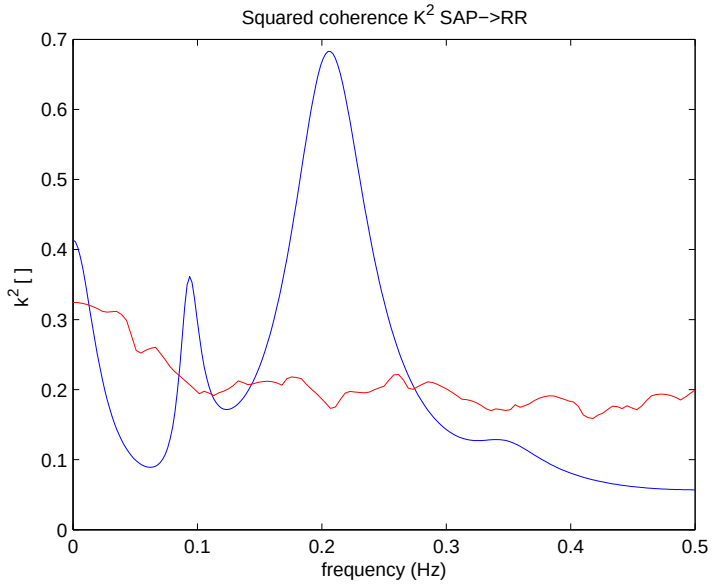

(a) $k^2_{SAP\rightarrow RR}$ (blue line) and $T(f)$ (red line)

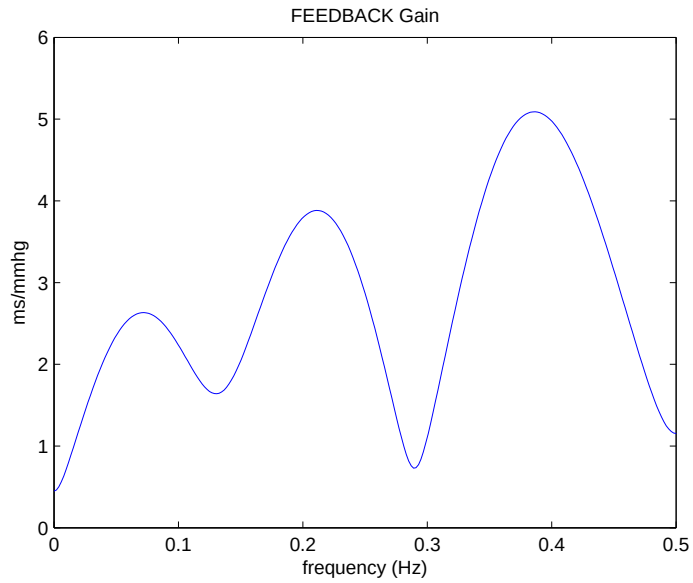

(b) $G_{SAP\rightarrow RR}$

Figure 2.5: In the upper panel, an example of casual feedback coherence (blue line) is reported with the threshold (red line) expressed as function of frequency through the surrogates method. In the lower panel, an example of baroreflex transfer function is reported.

2.2.6 Granger causality test

A time series $u = \{u(n), n = 1, \ldots, N\}$ is said to Granger-cause the series $y = \{y(n), n = 1, \ldots, N\}$, if the knowledge of a certain number of past values of y and u are more helpful to predict y than the exclusive knowledge of past values of y [66], [67]. Assuming that variables u and y are stochastic and stationary, Granger causality can be assessed by the F-test [67], [10], that verifies if an ARX model with exogenous input u is better fits and explains better y than a simple AR model. The AR model on y is defined as

$$y(n) = A_{yy}(z)y(n) + w_y(n) \tag{2.15}$$

with

$$A_{yy}(z) = \sum_{i=1}^{na} a_{yy,i} z^{-i}$$

where na is the model order and λ^2_{AR} is the variance of the input white guassian noise (WGN). While the ARX model on y is defined as

$$y(n) = A_{yy}(z)y(n) + B_{yu}(z)u(n - nk) + v_y(n) \tag{2.16}$$

with

$$B_{yu}(z) = \sum_{i=0}^{nb} b_{yu,i} z^{-i}$$

where nb is order of the exogenous part, nk is the input delay and λ^2_{ARX} is the variance of the input WGN. The ability of the models to fit is measured according to the means squared prediction error (MSPE)

$$\hat{\lambda}^2 = \frac{1}{N} \sum_{n=1}^{N} e^2(n|n-1) \tag{2.17}$$

where

$$e(n|n-1) = y(n) - \hat{y}(n|n-1)$$

It is important to notice that in case of AR model

$$\hat{y}(n|n-1) = \hat{A}_{yy}(z)y(n) \tag{2.18}$$

whilst in ARX model

$$\hat{y}(n|n-1) = \hat{A}_{yy}(z)y(n) + \hat{B}_{yu}(z)u(n - nk) \tag{2.19}$$

According to the system identification theory [66], $\hat{\lambda}^2$ is also an estimate of the variance of the input WGN. The null hypothesis is that the ARX model

does not reduce the MSPE with respect to the AR model. The following an F distribution is used as statistical distribution to test this hypothesis:

$$F = \frac{(\hat{\lambda}^2_{AR} - \hat{\lambda}^2_{ARX})}{\hat{\lambda}^2_{ARX}} \frac{(N - na - nb - 1)}{nb + 1} \tag{2.20}$$

where na is the AR model order, nb is the model order of the exogenous part and N is the signal length. The calculated F value is compared with the critical value of the F distribution with $(nb+1,\ N-na-nb-1)$ degrees of freedom derived for a given type-I error probability. In case F is larger, the null-hypothesis is rejected and a significant causal relationship between u and y is accepted. Both feedback and feedforward pathways are tested: in the former case the exogenous input is SAP, in the latter RR series. The order of the models are equal to $p = 8$ and the coefficients were estimated with LS method.

It is important to notice that Granger test is a pivotal step to confirm the presence of significant relationship between RR and SAP. Indeed, even though the coherence in the different frequency band can be very low, this causality test justifies the reasonability to estimate the BRS. The Granger test is performed for each phase both for *feedback* and *feedforward* mechanisms, with type-I error equal to 0.05.

2.2.7 Impulse response analysis

The minimal closed-loop model reported in Figure 2.3 and described by (2.5) can actually be written in time-domain as difference equations

$$RR(n) = \sum_{m=0}^{M-1} h_{ABR}(m) \cdot SAP(n - m - T_{ABR}) + w_{RR}(n) \tag{2.21}$$

$$SAP(n) = \sum_{m=0}^{M-1} h_{CID}(m) \cdot RR(n - m - T_{CID}) + w_{RR}(n) \tag{2.22}$$

where $h_{ABR}(m)$ and $h_{CID}(m)$ represent respectively the impulse response of the arterial baroreflex (ABR) or *feedback* mechanism (Figure 2.3) and the impulse response of the circulatory dynamics (CID) or *feedforward* mechanism [42]. By definition, the impulse response provides a complete characterization of the dynamics properties of the system, since the response of this system to any arbitrary input can be predicted by mathematically convolving the input with the impulse response [44]. For instance, $h_{ABR}(m)$ quantifies the time course of the change in RR series from an abrupt increase

in SAP of 1 $mmhg$. The linear systems theory states that $h_{ABR}(m)$ can be estimated as the inverse of *discrete Fourier transform* (DFT) of $G_{SAP \to RR}$. According to Marmarelis [68], the impulse response can be also expanded in a sum of weighted Laguerre basis functions:

$$h(m) = \sum_{j=0}^{q-1} c_j b_j(m) \tag{2.23}$$

where $b_j(m)$ represents the jth-order discrete time orthonormal Laguerre function and c_j are the corresponding unknown weights that are assigned to $b_j(m)$ in $h(m)$. If we name $x(n)$ as input and $y(n)$ as output, the (2.21) and (2.22) can be rewritten in the form

$$y(n) = \sum_{j=0}^{q-1} c_j v_j(n) \tag{2.24}$$

where

$$v_j(n) = \sum_{m=0}^{M-1} b_j(m) x(n-m) \tag{2.25}$$

According to (2.24), the expansion coefficients c_j can be estimated through multiple regression of y on the multinomial terms composed of the known functions $b_j(m)$. This method presents many advantages compared with bivariate model:

- The impulse response is finite to a number of coefficient M, that is defined as the *system memory*, while the inverse DFT of $G_{SAP \to RR}$ is infinite [69].

- This method computationally *opens the loop* of the closed-loop system (Figure 2.3), thereby separating the feedforward from the feedback components, but respecting the baroreflex causal structure. Indeed, the transfer function in equation (2.3) expresses only a degree of correlation in the frequency domain, but it cannot guarantee the causal relation between SAP and RR. On the opposite, the two sets of equations (2.21) and (2.22) can completely described the physiological HRV and *arterial blood pressure variability* (APV).

- The usage of Laguerre functions reduces the number of unknown "parameters" to estimate from M to q, reducing the computational burden compared to inverse DFT.

- This approach is considered *non-parametric* because it does not require any model $M(\theta)$ that regulate the relationship between SAP and RR, as in bivariate ARX model. On this perspective, the impulse response approach is another method to investigate the baroreflex function.

In this research study, the ABR impulse response is described through the peek-to-peek magnitude and the peek-delay, in order to understand the intensity and the speed of action of the ABP regulation mechanism. An example of ABR is reported in Figure 2.6.

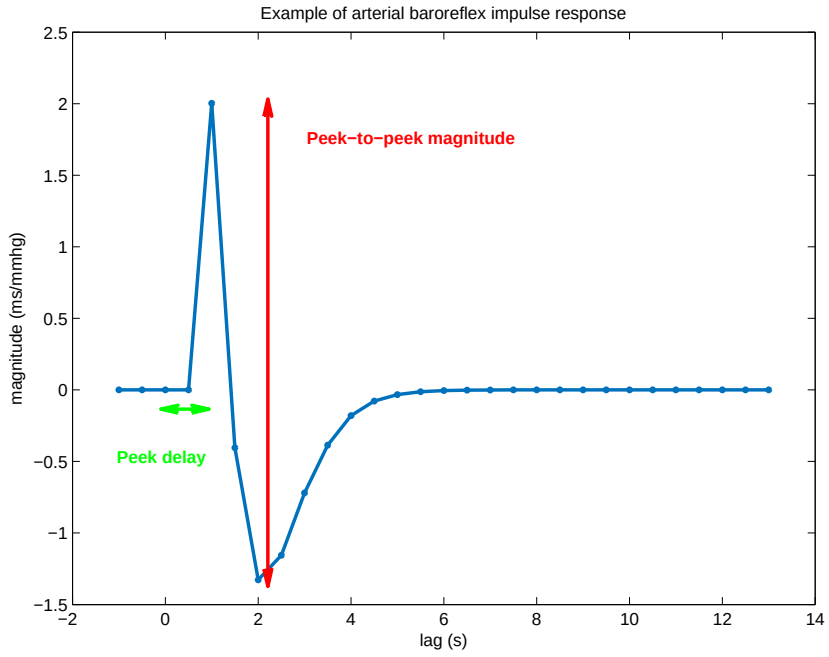

Figure 2.6: An example of h_{ABR} is shown.

2.2.8 Coefficient of sample Entropy

Alongside the study of baroreflex and other linear measures, this study includes also some nonlinear indexes from nonlinear theory. The heart and the cardiac regulation are considered a *low-order chaotic* system, whose complexity is an "index of health" [70]. In fact, a reduction or a modification of the non-linear interactions within and among signals are frequently exploited to diagnose pathologies, outcome mortality and impairing states [71],

[72], [73]. In this research, *the coefficient of sample entropy* ($COSEn$) is employed to study RR intervals during the different phases of the experimental protocol to complete the analyses and to contribute in the interpretation of the results coming from the baroreflex analysis. $COSEn$ is an entropy estimator and has been proposed to correct flaws and drawbacks in *sample entropy* ($SampEn$) [74]. The concept of Entropy was defined by Shannon [75], but it was further studied by Kolmogorov and others [76], [77]. Moorman [72] defined $SampEn$ to overcome the limits of *approximate entropy* ($ApEn$), defined by Pincus [78] to measure entropy in biological signal. The entropy measures the irregularity of a signal, such as a RR series, to detect atrial fibrillation (AF) [71], [74]. On this perspective, $SampEn$ is conceived as the conditional probability that two short templates match with an arbitrary tolerance will continue to match at the next point. Given a data record of N samples $\mathbf{X} = \{x_1, x_2, \ldots, x_N\}$, a length $m < N$ and starting point i, $\mathbf{x}_m(i)$ is a vector of m consecutive samples of the $\mathbf{X}$ series, i.e. $\mathbf{x}_m(i) = \{x_i, x_{i+1}, \ldots, x_{i+m-1}\}$. For a matching tolerance $r > 0$, a template match occurs when the distance between $\mathbf{x}_m(i)$ and another template at point j $\mathbf{x}_m(j)$ is inferior to r [72]. Let denote B_i the number of matches of length m within template $\mathbf{x}_m(i)$ and A_i denote the number of matches of length $m+1$ within template $\mathbf{x}_{m+1}(i)$. $A = \sum_i A_i$ and $B = \sum_i B_i$ are defined respectively as the total number of the matches of length $m+1$ and m. The ratio $cp = A/B$ is the conditional probability that subsequent points of a set of closely matching m intervals also remain close. The sample entropy is the negative natural logarithm and it is computed as:

$$SampEn = -ln(cp) = -ln(A/B) = -ln(A) + ln(B) \tag{2.26}$$

In regular series, cp tends to be close to 1 because templates are regular and the number of matches are similar regardless its size m. On the opposite, chaotic series have very low cp because templates are irregular. Irregular signals have high entropy, while regular signals have low entropy. Even though $SampEn$ is recognized to be less dependent on time series length and presents relative consistency on wider range of parameters, as tolerance, $SampEn$ is function of m and r and the choice of these parameters can affect the reliability of the cp estimation. On one hand, large value of m or small value of r leads to a small number of matches, insufficient for confident results. On the other one, a small m or a large r increase excessively the number of template matches, without any differentiations among rhythms. On this perspective, Lake proposed the quadratic sample entropy (QSE) [72], that consists in $sampEn$ normalized by the volume of each matching region, $2r^m$. According to definition of QSE, the 2.26 is rewritten in the

following form

$$QSE = -ln(cp) + ln(2r) = SampEn + ln(2r) \tag{2.27}$$

Starting from 2.27, $COSEn$ is defined as

$$COSEn = SampEn + ln(2r) - ln(\overline{RR}) \tag{2.28}$$

where $\overline{RR}$ stands for the average of the considered RR segment as well as the average of the signal considered. This factor is added due to its importance to predict AF, as shown in Moorman [74]. Furthermore, $COSEn$ has the power to predict AF even in short segments. In this study, the parameters m and r were set equal to 1 and 30 ms respectively [74].

In addition to $COSEn$, the *local dynamics score* (LDS) is computed for each phase. The LDS is a new index to investigate the local dynamics of short RR series [79]. The innovative idea is to examine how often individual templates in a short series match each other not only according to the rhythm, but also according to the local dynamics of the signal. In the original work the authors examined the challenging situation of the coexistence of reduced heart rate variability (HRV) and ventricular ectopy. Given a 12-beat segment, the algorithm consists mainly into counting the number of times each sample matches with the other 11 with a tolerance r of 20 msec. A histogram of the count of templates as a function of the number of matches is constructed. If no points match, a bar of 12 counts appears in the bin 0, and all the other bins are empty, when all 12 points match each other, the histogram will have a bar of 12 counts in bin 11. The LDS is computed as a linear combination of the values in bin 0, bin 10 and bin 11; the coefficients were normalized so as to sum to 1. A uniform distribution of matches, i.e. the counts in all bins are equal to 1, leads to LD score of 1. Lower scores imply a bell-shape histogram distribution, and higher scores imply a distribution concentrated on either or both extremes of the histogram.

2.3 Data analysis

2.3.1 Data pre-processing and segment detection

The recorded signals are subdivided into five epochs: the first one is the pre-cardiac arrest (Pre-CA) phase, that occured before the CA, but after the anesthesia induction, that's why we could not consider it as a baseline.

The others consist in post-resuscitation phase after 1 h, 2 h, 3 h, 4 h. For each phase, a window of ABP with a length ranging from 10 to 15 mins is extracted. The exact time location of the window is defined both in qualitative and quantitative manner within each phase. After a manual selection of stationarity subsequences, the time series are then subsequently evaluated by a "beat-by-beat" quality algorithm, whose task is to count how many ABP waves were suitable for successive analyses. The windows are finally chosen maximizing the percentage of "good beats",at least a percentage greater than 80%. Each window is divided in 50% overlapping shorter segments of 180 s. A robust algorithm is employed for detection of the onset of each beat. The algorithm converted the signal in a slope sum function, which amplifies the rising part of ABP waveform in each beat [80]. Each time-location onset is found through, first, an adaptive thresholding and, second, a local search strategy around the previous fiducial point detected. SAP and DAP are recognized respectively as the local maximum and minimum in each time window following the onset. The pulse pressure (PP) is estimated as the difference between SAP value of the current cardiac cycle and DAP value of the previous cycle. The RR interval is estimated by considering the heart period (HP), that is the difference of two consecutive ABP onsets, as the pressure slope occurred co-currently with R peaks of ECG. Hence, HP has equivalent physiological meaning of the QRS time occurrences difference. Thanks to this procedure, beat-by-beat series of the major cardiovascular variables are obtained. The series are pre-processed with an adaptive filter [81] in order to remove artifacts and/or ectopic beats. Each variable is then demeaned and detrended.

Beat-by-beat series are resampled at 2 Hz to perform spectral analysis. Autoregressive estimation is chosen to compute power spectral density (PSD). Powers in very low frequency band (VLF, 0-0.04 Hz), low frequency band (LF, 0.04-0.15 Hz) and high frequency band (HF, 0.15-0.4 Hz) are computed as follows

$$Power([f_1, f_2]) = \int_{f_1}^{f_2} PSD(f)df \tag{2.29}$$

The values of total power are computed as well with (2.29), considering the entire band till the Nyquist frequency. The normalized power is computed in LF and HF band according to following equations:

$$LF(\%) = \frac{P(LF)}{P([0, f_{nyquist}]) - P(VLF)} \cdot 100 \tag{2.30}$$

$$HF(\%) = \frac{P(HF)}{P([0, f_{nyquist}]) - P(VLF)} \cdot 100 \tag{2.31}$$

AIC is exploited to find the optimal model order, which is set to be in a range between 8 and 12.

For each time series (RR, SAP, DAP, PP) the mean and standard deviation are assessed.

2.3.2 Statistical analysis

Each index or estimation are calculated for each subsegment within any phase. The median values are extracted to represent each phase of any pig and these values are used for comparisons purpose. The data are represented as mean ± SD for each experimental phase as well as separately for the argon and the control groups. In contrast, the figures reports the indexes values as mean±SE, where SE is *standard error* and is computed as $SE = \frac{SD}{\sqrt{N}}$, with N equal to the number of pigs. The p-values of the Granger causality test are reported for each phase of any pig. Indeed, the number of positive tests are simply counted and the single values were plotted.

A one way repeated measures ANOVA is performed for each index, with experimental epochs being the repeated factor. Post-hoc comparisons are performed using the paired Student's t-test in order to verify significant differences among the different post-resuscitation periods with respect to the pre-cardiac arrest epoch. Unpaired two-sample Student's T-test is used to compare values from argon and control pigs for each epoch (pre-CA and post-resuscitations epochs) in order to verify the effects of Argon ventilation with respect to common ventilation technique. A two tailed p-value less than 0.05 is considered statistically significant.

Chapter 3

Results

3.1 Changes after CA

The main characteristics of the two animal groups are previously reported in Table 2.1. In the first part of the chapter, an overall analysis of all animals is discussed. It is important to highlight that all pigs successfully survived the CPR.

3.1.1 Cardiovascular changes in time-domain

In this section, a time-domain overview of the analyzed signals is described. An example of the time course of the main cardiac and hemodynamic variables during the different experimental epochs is displayed in the left panels of Figure 3.1 and Figure 3.2. In Table 3.1, the moments of the first and second order of the series are reported.

After CA, the mean RR decreases without a recovery as well as PP, as already reported in [5] (Table 3.1). The absence of the PP recovery is in line with the fact that the cardiac output is not restored after the experiment and, indeed, the pulse pressure can be considered as a surrogate of *stroke volume* (SV). In contrast, the SAP and DAP mean values diminish after CA and then rise within 4 hours of the experiment, returning to values similar at pre-cardiac arrest (Pre-CA).

Both RR and pressure variables present differences that are statistical significant among the experimental epochs. Furthermore, RR and PP do not recover after CA and their values are significantly different between Pre-CA and all other phases. In contrast, SAP and DAP increase with time course of the experiment, i.e. after resuscitation. In particular, SAP and

DAP reach the pre-CA values at Pr 3h and Pr 4h: the values of Pre-CA vs Pr 1h, Pr 2h are significantly higher as well as the values of Pr 3h, Pr 4h vs Pr 1h, Pr 2h are significantly higher, as reported in Table 3.1.

The standard deviation of RR seems to show the same pattern of SAP and DAP mean values. In particular, the values of RR standard deviation significantly decrease and after CA and then they return to values similar to pre-CA (no significant differences). In contrast, all the other standard deviations do not exhibit significant changes with the experimental epochs.

The values of nonlinear indexes for RR are reported in Table 3.2. A significant increase of $COSEn$ values is found in the experimental epochs after resuscitation with respect to pre-CA values. According to Moorman [74], such increase hints a more regular rhythm, that is typical of some cardiovascular pathology, as in case of regular premature ventricular contractions such as bigeminy, or some heart electrical instability. Moorman [74] defined heart rhythms which are likely to develop AF if $COSEn$ is higher than an empirical threshold equal to -1.4. Although the index in each phase is not greater than -1.4 , its increase in post-resuscitation could suggest a condition or a propensity to electrical instability.

Time-domain indexes	Pre-CA	Pr 1h	Pr 2h	Pr 3h	Pr 4h	RM ANOVA
RR mean ms	621.85±139.9	438.48±108.41 §	434.62±75.01 §	460.19±101.79 §	443.36±76.03 §	$p \leq 0.01$
RR SD ms	9.78±7.42	4.52±2.12 §	6.01±1.79	5.63±2.54	6.06±2.23	$p \leq 0.05$
SAP mean $mmhg$	118.57±13.50	98.42±12.90 §	107.42±12.13 §	110.73±14.02 ‡	111.63±13.23 ‡ #	$p \leq 0.01$
SAP SD $mmhg$	3.19±1.22	2.83±1.11	2.98±0.88	3.10±1.57	3.08±1.42	$n.s.$
DAP mean $mmhg$	95.12±11.10	79.80±14.31 §	90.00±13.43	93.15±14.48 ‡	93.74±13.26 ‡ #	$p \leq 0.01$
DAP SD $mmhg$	2.44±1.12	2.41±1.02	2.55±0.80	2.82±1.63	2.81±1.39	$n.s.$
PP mean $mmhg$	23.48 ± 4.26	18.53±3.22 §	17.47±3.61 §	17.67±4.02 § ‡	17.80±3.54 §	$p \leq 0.01$
PP SD $mmhg$	1.65±0.60	1.31±0.62	1.28±0.51	1.25±0.67 § #	1.26±0.55	$n.s.$

Table 3.1: The moments of first and second order of each data series are reported as mean± SD in any experimental phase. In the last column the p-value of the repeated measures *ANOVA is shown. The symbols §,‡,# represent significant post-hoc comparisons vs Pre-CA, Pr 1h, Pr 2h epoch, respectively.*

Complexity indexes	Pre-CA	Pr 1h	Pr 2h	Pr 3h	Pr 4h	RM ANOVA
RR LD score	1.38±0.54	1.71±0.02 §	1.72±0.03 §	1.73±0.07 §	1.74±0.05 §	$p \leq 0.01$
RR COSEn	-2.13±0.23	-1.81±0.21	-1.81±0.16 ‡	-1.85±0.22	-1.82±0.16 ‡	$p \leq 0.01$

Table 3.2: The LDS and $COSEn$ for RR intervals are reported as mean± SD in any experimental phase. In the last column the p-value of the repeated measures *ANOVA is shown. The symbols §,‡,# represent significant post-hoc comparisons vs Pre-CA, Pr 1h, Pr 2h epoch, respectively*

3.1.2 Cardiovascular autonomic response in frequency domain

In this section, a frequency-domain overview of the cardiovascular signals is reported. The right panels of Figure 3.1 and Figure 3.2 show an example of the power spectral densities of the following time series: RR intervals, systolic arterial pressure, diastolic arterial pressure and pulse pressure in the different experimental epochs. Table 3.3 reports the main spectral indexes of HRV as suggested in the European Task Force of Cardiology [23], as well as the spectral indexes of blood pressure, which are:

- the average power of the variables in the LF, VLF and HF band, according to (2.29)
- the total power of the signals
- the LF and HF power expressed in normalized unit, according to (2.30)

The absolute RR power in LF band shows a decreasing trend after CA with a recovery in the following resuscitation period, even though the values are not significant. Similarly the absolute PP power in LF band show a drop after CA without recovery. In similar way, LF components of SAP and DAP suggest a u shape in the observed time period.

Although animals are mechanically ventilated and there is an ongoing respiratory entrainment mechanism, HF components are compared. RR power in HF band changes significantly during the different experimental epoch (see Figure 3.3). Furthermore, HF values of pre-CA are significantly higher than the values at Pr 1h, Pr 2h, as reported in Table 3.3, and the values during the last two hours of the experiment are significantly higher with respect to the first two post-resuscitation hours as reported in Table 3.3 and in Figure 3.3. On the opposite, the HF components of the other blood pressure variables do not show any significant change over time and they remain stable. This is also consequence of the fact that HF components in SAP, DAP and PP do not represent any autonomic response, but only the respiratory effect that occur on vessels.

If we consider the normalized power of LF and HF spectral components, no significant differences are obtained among the considered epochs. In general, we can observe that the normalized power in HF band is always greater than the normalized power in LF band and this is not surprising as the animals are mechanically ventilated.

A global measure of variability is the total power of the different variables. RR total power diminishes after the onset of the impairing condition and recovers in the following post-resuscitation epochs, as shown in Table 3.3 and in Figure 3.3. In fact, the values measured at Pr 4h versus Pr 1h and Pr 2h are significantly higher. On the opposite, the total power of SAP, DAP and PP do not show any particular pattern.

Frequency-domain indexes	Pre-CA	Pr 1h	Pr 2h	Pr 3h	Pr 4h	RM ANOVA
RR intervals						
RR Power(LF) (ms^2)	19.13±36.37	1.76±1.62	2.51±2.85	4.26±4.42	4.66±4.28	$n.s.$
Normalized RR Power (LF) (%)	33.49±30.87	29.19±8.37	29.68±12.38	33.09±6.20	32.74±9.79	$n.s.$
RR Power (HF) (ms^2)	16.40±22.35	2.69±2.02	3.43±2.80 ‡	5.75±5.31 #	5.93±5.55 ‡ #	$p \leq 0.05$
Normalized RR Power (HF) (%)	54.14±28.86	46.81±6.01	47.84±10.34	46.62±5.66	45.88±9.99	$n.s.$
RR power(VLF) (ms^2)	4.58±3.48	2.52±2.50	4.27±3.38	3.57±3.16	3.56±3.19	$n.s.$
Total RR power (ms^2)	44.73±48.47	8.61±6.15 §	12.64±7.99 §	16.43±12.75	16.94±13.30 ‡ #	$p \leq 0.01$
SAP						
SAP Power(LF) ($mmhg^2$)	1.21±2.12	0.50±0.47	0.51±0.48	1.27±1.52	1.16±2.10	$n.s.$
Normalized SAP Power(LF) (%)	35.84±39.38	19.96±13.61	21.46±16.76	36.62±27.64	31.44±24.69	$n.s$
SAP Power(HF) ($mmhg^2$)	1.41±1.89	2.05±2.43	1.77±0.95	1.94±2.97	3.02±5.25	$n.s.$
Normalized SAP Power(HF) (%)	62.02±39.15	70.73±13.82	73.72±18.08	57.78±26.13	62.35±24.45	$n.s.$
SAP Power(VLF) ($mmhg^2$)	0.25±0.22	0.29±0.21	0.59±0.50	1.34±3.13	1.36±2.92	$n.s.$
Total SAP power ($mmhg^2$)	6.78±6.36	4.49±3.71	4.37±2.11	6.07±7.51	5.36±5.61	$n.s.$
DAP						
DAP Power(LF) ($mmhg^2$)	3.87±6.91	0.48±0.55	0.51±0.43	0.98±1.13	1.06±2.08	$n.s.$
Normalized DAP Power(LF) %	35.03±42.39	13.68±14.12	16.54 ±15.13	28.59 ±27.18	24.95 ±24.75	$n.s.$
DAP Power(HF) ($mmhg^2$)	2.28±2.50	3.12±3.08	2.93±1.90	3.39±5.78	2.79±3.04	$n.s.$
Normalized DAP Power(HF) %	62.62±41.14	73.46±13.59	78.98±16.61	67.00±26.28	69.25±24.31	$n.s.$
DAP Power(VLF) ($mmhg^2$)	0.28 ±0.18	0.28±0.21	0.62±0.56	1.35±3.51	1.40±2.92	$n.s.$
Total DAP power ($mmhg^2$)	2.99±2.65	3.04±2.90	3.06±1.24	4.97±6.27	5.69±6.67	$n.s.$
PP						
PP Power(LF) ($mmhg^2$)	0.86±1.38	0.10±0.07	0.08±0.07	0.15±0.19	0.13±0.11	$n.s$
Normalized PP Power(LF) (%)	34.43±38.93	13.88±6.82	12.72±7.98	21.97±14.88	18.77±10.05	$n.s.$
PP Power(HF) ($mmhg^2$)	0.64±0.44	0.72±0.95	0.63±0.53	0.63±0.75	0.59±0.56	$n.s.$
Normalized PP Power(HF) %	61.77±37.94	67.14±15.41	75.58±11.89	67.23±15.27	67.63±14.28	$n.s.$
PP Power(VLF) ($mmhg^2$)	0.28±0.18	0.28±0.21	0.62±0.56	1.35±3.51	1.40±2.92	$n.s$
Total PP power ($mmhg^2$)	1.72±1.45	1.04±1.12	0.84±0.65	1.00±1.13	0.98±0.76	$n.s.$

Table 3.3: The absolute and relative powers of each data series in HF, LF and VLF bands are reported as mean± SD in any experimental phase. In the last column the p-value of the repeated measures *ANOVA is shown. The symbols §,‡,# represent significant post-hoc comparisons vs Pre-CA, Pr 1h, Pr 2h, respectively.*

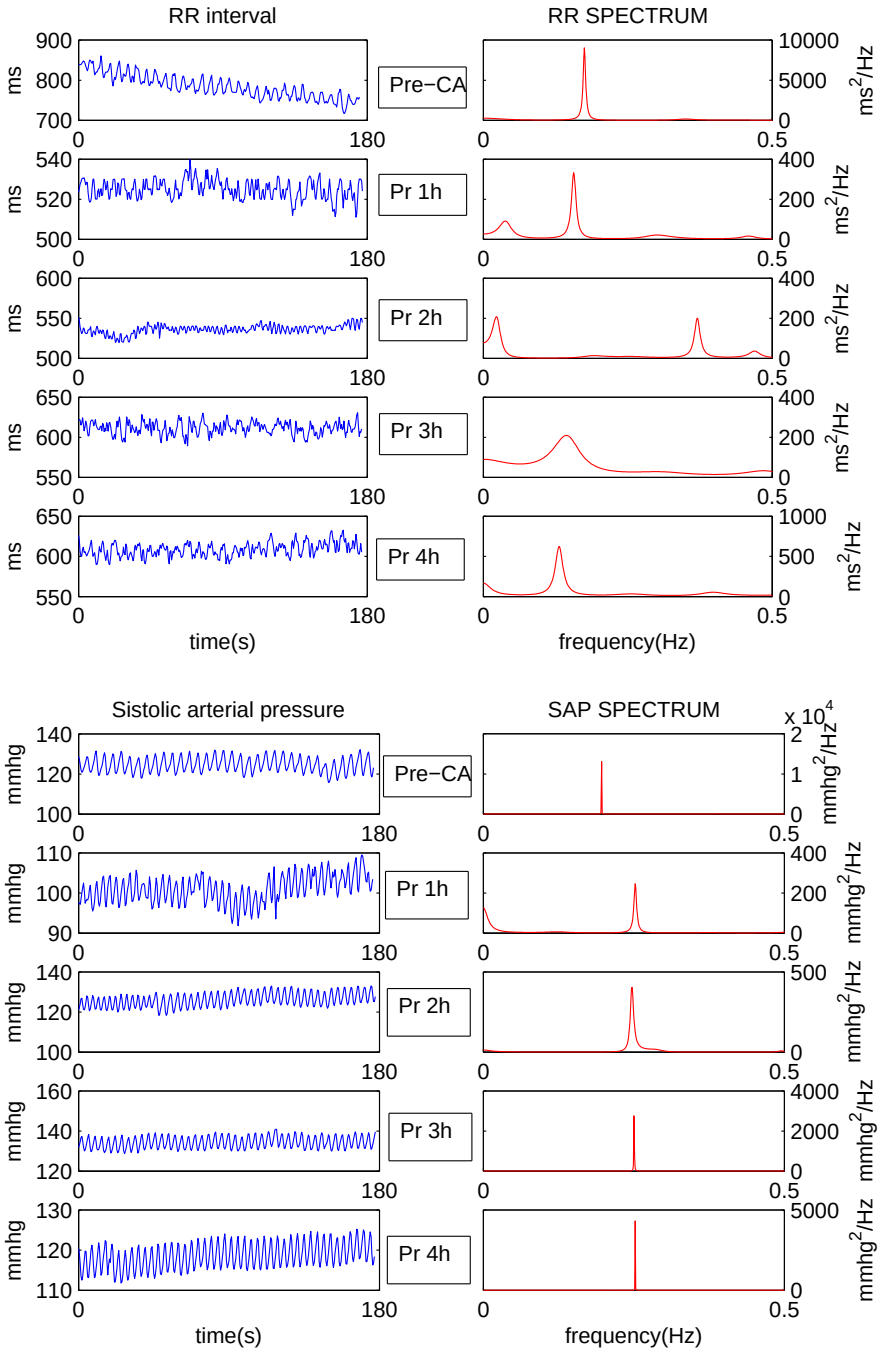

Figure 3.1: The left panels show the time series at the different experimental epochs, whereas the right panels illustrate the associated spectra

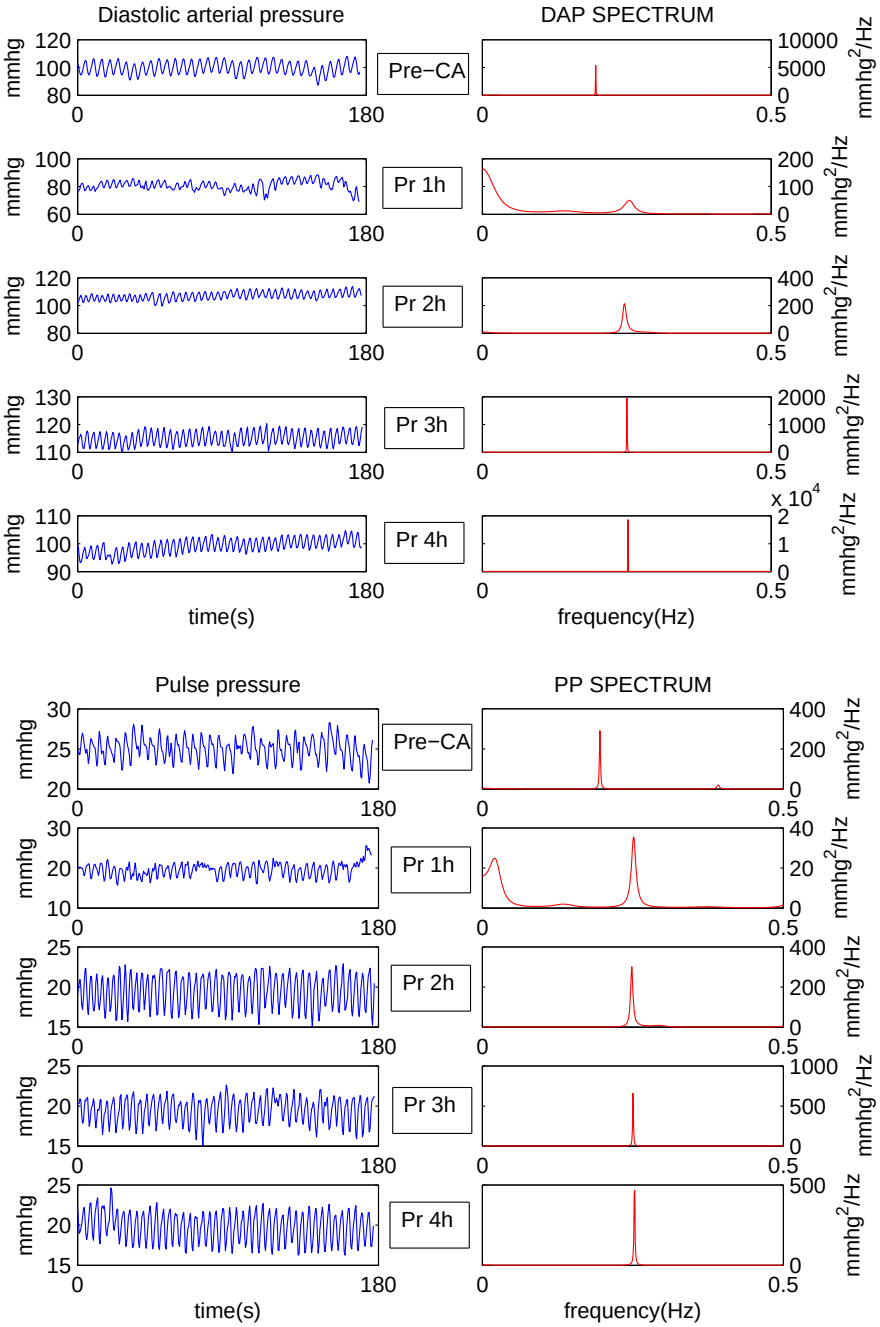

Figure 3.2: The left panels show the time series at the different experimental epochs, whereas the right panels illustrate the associated spectra

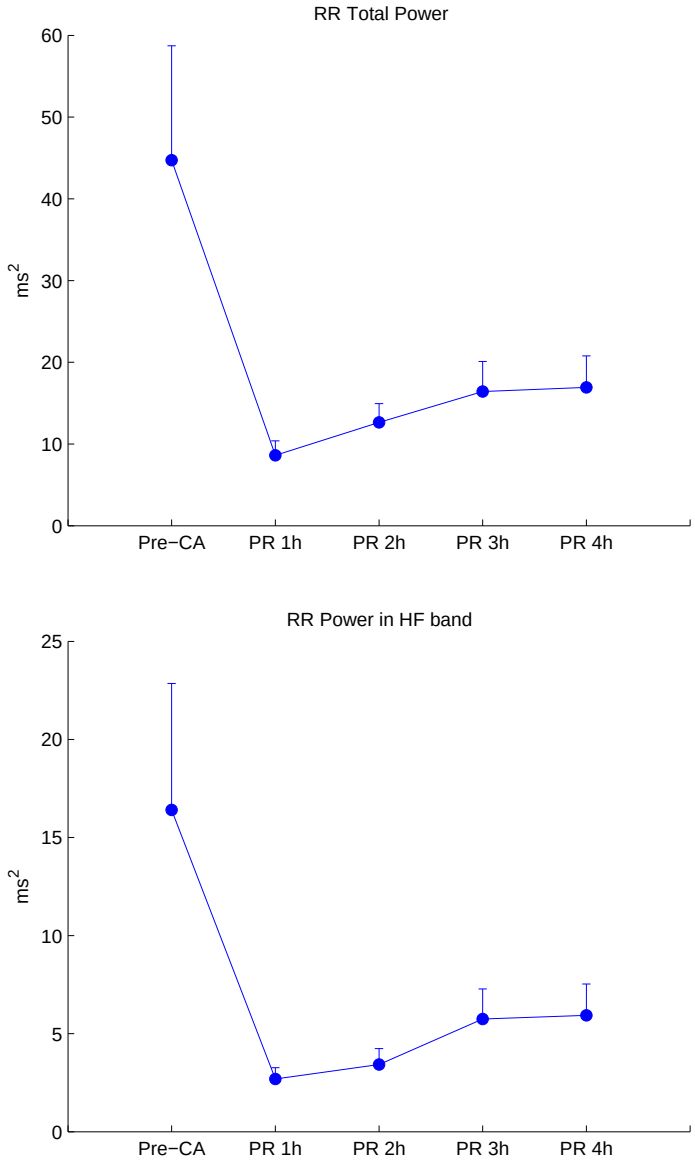

Figure 3.3: In the upper panel, the evolution of RR total power expressed as mean+SE is shown. In the lower panel, the attention is focused on RR power in HF band.

3.1.3 Granger causality test

In Figure 3.4, p-values of the Granger test for the *feedback* relationship, i.e. the results of the test on the causality of SAP oscillations on RR changes, are reported for each pig in each experimental phase. The number of pigs that fulfill test are reported in Table 3.4. If the type-I error is equal to 0.05 (green line in Figure 3.4), most of the pigs present a significant ARX relation in each phase. There are some pigs that do no reject the null-hypothesis, although there are p-values slightly over the threshold. In general, it can be said that pigs tend to present a significant relation in every epochs.

In Figure 3.5, p-values of the Granger test for the *feedforward* relationship, i.e. the results of the test on the causality of RR oscillations on SAP changes. The number of pigs that fulfill the test are listed in Table 3.4. Even though most of the pigs present p-values less than 0.05, there is a strong reduction of the number of pigs during phase Pr 2h and Pr 3h compared with the *feedback* mechanism, as shown in Table 3.4.

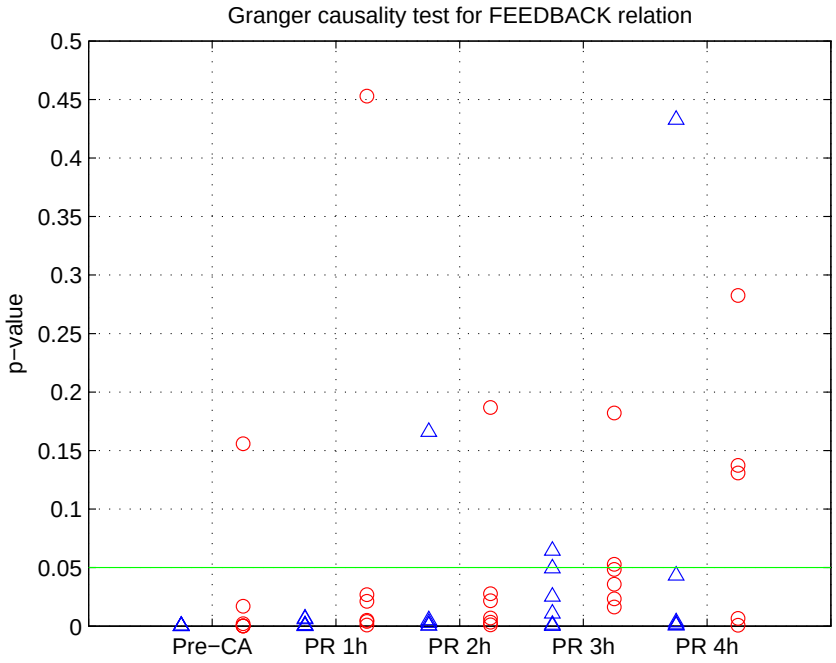

Figure 3.4: The blue triangles represent the p-values of the control pigs for the Granger causality test, while the red circles represent the p-values of argon group. The green line defines the threshold level equal to 0.05.

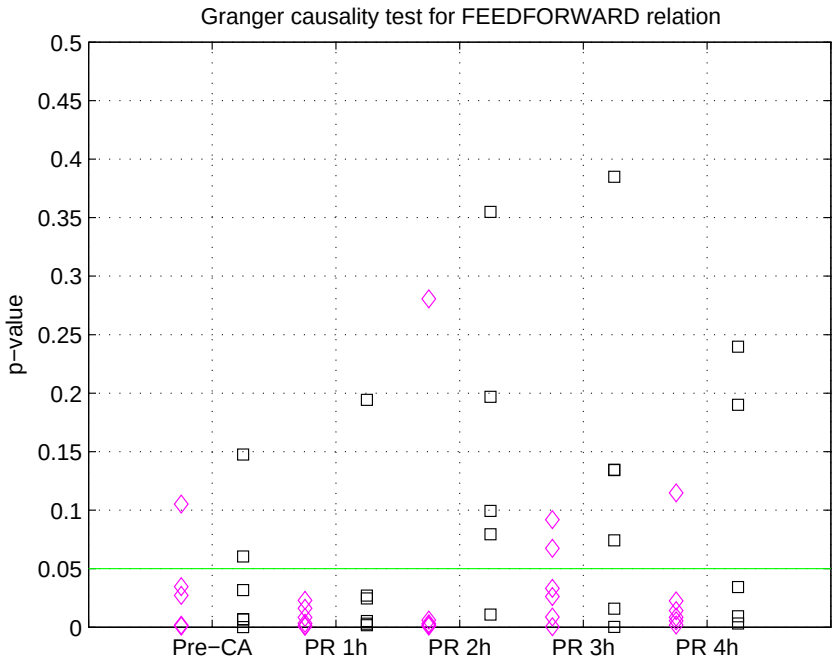

Figure 3.5: The magenta diamonds represents the p-values of the control pigs for the Granger causality test, while the black squares represent the p-values of argon group. The green line defines the threshold level equal to 0.05.

3.1.4 Baroreflex indexes and coherence analysis

The mean values of the BRS are reported in Table 3.5. They are indicated with the greek letter α as commonly reported in literature [48], [3], [63]. The α_{PR} stands for the baroreflex gain computed with power ratio as described in equation (2.1), while α_{CS} is computed with non-parametric cross-spectrum analysis with the mathematical equation (2.3). The $\alpha_{SAP \to RR}$ is the gain obtained from the bivariate model (see §2.2.5) . The BRS estimates have different ranges of values according to the applied methods, in particular the BRS values estimated by the bivariate model has the lowest ones, as expected [48]. Furthermore, $\alpha_{SAP \to RR}$ in HF tends to be greater than $\alpha_{SAP \to RR}$ in LF, with both the approaches, as reported in Table 3.5. On the opposite, α_{PR} and α_{CS} present similar value in the two frequency bands. The insurgence of the cardiac arrest generates a drop of the baroreflex gain values with a following partial recovery in the post-resuscitation. The values in pre-CA epoch are significantly higher than values at Pr 1h and Pr 2h, as well as Pr 3h and Pr 4h values are significantly greater than

Number of positive Granger tests	Pre CA	Pr 1h	Pr 2h	Pr 3h	Pr 4h
Feedback					
All pigs	11/12	11/12	10/12	9/12	7/12
Argon	5/6	5/6	5/6	4/6	2/6
Control	6/6	6/6	5/6	5/6	5/6
Feedforward					
All pigs	9/12	11/12	6/12	6/12	8/12
Argon	4/6	5/6	1/6	2/6	3/6
Control	5/6	6/6	5/6	4/6	5/6

Table 3.4: Number of the Granger tests are reported, either both for all pigs and divided in the two experimental groups. It is interesting to notice the reduction of passed tests in the Pr 3h and Pr 2h in the feedforward direction, i.e. relating to runoff mechanism.

values at Pr 1h and Pr 2h, as reported in Table 3.5. The other estimators do not show significant differences across the experimental epochs. However, their trend suggests a partial recovery of the BRS, as shown by the increase of the BRS gain values after resuscitation and the reduction of the average differences of BRS values in the last hours of post resuscitation period with respect to the values in the Pre-CA (Table 3.6). However, at the end of the experiment, the Pr 4h values remain lower than values estimated before cardiac arrest. The values for BRS gain in LF band, computed both without applying a threshold on the cross-spectrum and with the surrogates method, are reported in Figure 3.6 and in Figure 3.7. It can be noticed a u shape trend which hints a partial recovery of BRS gain values.

For sake of completeness, the mean values of the *feedforward* gain $G_{RR\rightarrow SAP}$ and associated mean coherence values in LF and HF bands are reported in Table 3.8. They are indicated with the greek letter β as commonly reported in literature [48], [3], [63]. The coherence reported is computed only without thresholding coherence. $\beta_{RR\rightarrow SAP}$(LF) does not show any significant pattern over time. In contrast, $\beta_{RR\rightarrow SAP}$(HF) is significant greater in Pr 1h than all other phases. Figure 3.8 show $\beta_{RR\rightarrow SAP}$ in LF and HF band in the different experimental epochs without applying any threshold to the coherence associated.

The mean values of coherence between SAP and RR in the different experimental epochs are reported in Table 3.7. The parameter k^2_{CS} stands for the coherence computed with non-parametric cross-spectrum analysis, whilst k^2_{BIV} represents the coherence computed with (2.12), that is expres-

sion of the bivariate model, described in Chapter 2. The latter is also indicated as *closed loop* coherence, because it describes a generic degree of correlation between SAP and RR in the bivariate model and it does not highlight any lines of the block of Figure 2.3. In order to focus on the feedback block that receives SAP as input and RR as output, $k^2_{SAP \to RR}$ is reported in Table 3.7. All of these indexes is computed in the LF and HF bands. They all show a decrease of the coherence among the different experimental epochs with respect to Pre-CA epoch. The coherence computed with surrogates method is greater than values obtained with other method, because it considers values above the threshold to define the average. Furthermore, the coherence shown in the upper part of Table 3.7 are very low, because the method without applying a threshold on the coherence function involves samples with very low values in the considered band. The only method to estimate the coherence that shows significant differences over time is k^2_{CS} with the surrogates method. The lower part of the table justifies the use of the surrogates method. The average of the values greater than $T(f)$ in LF and HF band are below the common used threshold equal to 0.5. These results suggest that the coupling between SAP and RR is significant without having a coherence greater than 0.5.

BRS estimations	Pre-CA	Pr 1h	Pr 2h	Pr 3h	Pr 4h	RM ANOVA
Without thresholding coherence						
α_{PR}(LF) $ms/mmhg$	4.13±2.90	2.64±2.09 §	2.42±1.61 §	2.83±1.75#	3.26±2.12#	$p \leq 0.01$
α_{CS}(LF) $ms/mmhg$	3.26±2.04	1.74±1.70 §	1.42±0.56 §	2.01±1.13 § #	2.20±1.44 §#	$p \leq 0.01$
$\alpha_{SAP \rightarrow RR}$(LF) $ms/mmhg$	2.32±2.26	0.71±0.42 §	0.71±0.34 §	1.14±0.79 ‡ #	0.98±1.02	$p \leq 0.01$
α_{PR}(HF) $ms/mmhg$	3.22±3.50	1.34±1.41 §	1.22±0.83	1.91±1.37#	1.78±1.22#	$n.s.$
α_{CS}(HF) $ms/mmhg$	3.57±2.31	1.57±1.24 §	1.81±0.56 §	2.07±1.11	2.11±1.14	$p \leq 0.01$
$\alpha_{SAP \rightarrow RR}$(HF) $ms/mmhg$	1.97±1.03	1.05±0.67	1.07±0.43	1.26±0.73	1.37±1.34	$p \leq 0.05$
Surrogates						
α_{CS}(LF) $ms/mmhg$	4.12±3.29	1.95±1.96 §	1.75±0.87 §	2.26±1.21 § #	2.50±1.54#	$p \leq 0.01$
$\alpha_{SAP \rightarrow RR}$(LF) $ms/mmhg$	2.16±1.97	0.53±0.40	0.54±0.22	1.19±1.02	1.14±1.14	$n.s.$
α_{CS}(HF) $ms/mmhg$	3.48±3.33	1.80±1.51 §	2.06±0.65	2.35±1.31	2.41±1.32	$n.s.$
$\alpha_{SAP \rightarrow RR}(HF)ms/mmhg$	1.88±1.43	1.22±0.90	1.36±0.45	1.12±0.27	2.03±2.15	$n.s.$

Table 3.5: The BRS values expressed as mean± SD are reported for each experimental phase. The last column shows the p-value of the repeated measures *ANOVA. The symbols §,‡,# represent significant post-hoc comparisons vs Pre-CA, Pr 1h, Pr 2h, respectively.*

Absolute difference(Δ)	Pre-CA - Pr 1h	Pre-CA - Pr 2h	Pre-CA - Pr 3h	Pre-CA - Pr 4h
Without thresholding coherence				
α_{PR}(LF) $ms/mmhg$	1.48±2.02	2.15±1.97	1.12±2.37	0.65±1.76
α_{CS}(LF) $ms/mmhg$	1.51±1.73	2.02±1.87	1.19±1.40	0.95±1.17
$\alpha_{SAP \rightarrow RR}$(LF) $ms/mmhg$	1.63±2.03	1.70±2.25	1.14±2.21	1.27±2.42
α_{PR}(HF) $ms/mmhg$	1.86±2.31	2.06±3.32	1.27±3.11	1.40±3.51
α_{CS}(HF) $ms/mmhg$	2.04±1.44	1.83±2.08	1.47±1.94	1.43±2.10
$\alpha_{SAP \rightarrow RR}$(HF) $ms/mmhg$	1.01±0.83	0.94±1.09	0.70±0.96	0.52±1.49
Surrogates				
α_{CS}(LF) $ms/mmhg$	2.15±2.66	2.70±2.90	1.78±2.60	1.49±2.43
α_{CS}(HF) $ms/mmhg$	1.72±1.99	1.57±3.08	1.09±2.91	1.05±3.22

Table 3.6: The absolute differences among Pre-CA BRS values and the other phases are reported. Even though the values tend to decrease, the Δ remain positive in the last column, which underlines the BRS is not restored to the magnitude before the impairing conditions.

Coherence estimations	Pre-CA	Pr 1h	Pr 2h	Pr 3h	Pr 4h	RM ANOVA
Without thresholding coherence						
k^2_{CS}(LF)	0.39±0.22	0.40±0.12	0.35±0.14	0.42±0.16	0.35±0.12	$n.s$
k^2_{CS}(HF)	0.40±0.14	0.41±0.09	0.36±0.13	0.36±0.05	0.36±0.08	$n.s$
k^2_{BIV}(LF)	0.36±0.19	0.28±0.13	0.25±0.13	0.28±0.14	0.24±0.13	$n.s$
k^2_{BIV}(LF)	0.15±0.05	0.17±0.04	0.13±0.07	0.13±0.05	0.13±0.05	$n.s$
$k^2_{SAP\rightarrow RR}$(LF)	0.29±0.17	0.20±0.16	0.17±0.11	0.21±0.13	0.18±0.12	$n.s$
$k^2_{SAP\rightarrow RR}$(HF)	0.09±0.04	0.10±0.05	0.09±0.06	0.07±0.02	0.08±0.05	$n.s$
Surrogates						
k^2_{CS}(LF)	0.73±0.17	0.52±0.13	0.51±0.05 §	0.54±0.15 §	0.45±0.11 §	$p \leq 0.01$
k^2_{CS}(HF)	0.73±0.15	0.52±0.12 §	0.52±0.08 §	0.48±0.11 §	0.45±0.12 §	$p \leq 0.01$
$k^2_{SAP\rightarrow RR}$(LF)	0.63±0.19	0.46±0.09	0.49±0.12	0.42±0.08	0.39±0.17	$n.s$
$k^2_{SAP\rightarrow RR}$(HF)	0.49±0.31	0.33±0.13	0.36±0.10	0.31±0.05	0.28±0.08	$n.s$

Table 3.7: The coherence values expressed as mean± SD are reported in any experimental phase. The last column shows the p-value of the repeated measures *ANOVA. The symbols §,‡,# represent significant post-hoc comparisons vs Pre-CA, Pr 1h, Pr 2h, respectively.*

Feedforward gain values	Pre-CA	Pr 1h	Pr 2h	Pr 3h	Pr 4h	RM ANOVA
$\beta_{RR\rightarrow SAP}$ (LF) $mmhg/ms$	0.19±0.13	0.33±0.31	0.20±0.13	0.24±0.22	0.23±0.27	$n.s.$
$\beta_{RR\rightarrow SAP}$ (HF) $mmhg/ms$	0.06±0.04	0.11±0.05 §	0.06±0.03 ‡	0.08±0.06 ‡	0.07±0.05 ‡	$p \leq 0.01$
$k^2_{RR\rightarrow SAP}$(LF)	0.16±0.16	0.12±0.09	0.09±0.08	0.10±0.07	0.09±0.07	$n.s.$
$k^2_{RR\rightarrow SAP}$(HF)	0.07±0.03	0.08±0.03	0.06±0.03	0.07±0.05	0.07±0.04	$n.s.$

Table 3.8: The feedforward gains β expressed as mean± SD are reported in each experimental phase. The last column shows the p-value of the repeated measures *ANOVA. The symbols §,‡,# represent significant post-hoc comparisons vs Pre-CA, Pr 1h, Pr 2h, respectively.*

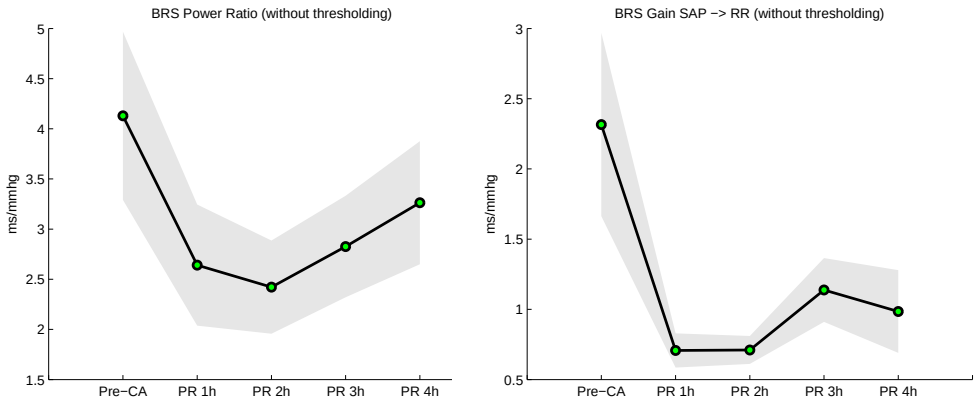

(a) *(b)*

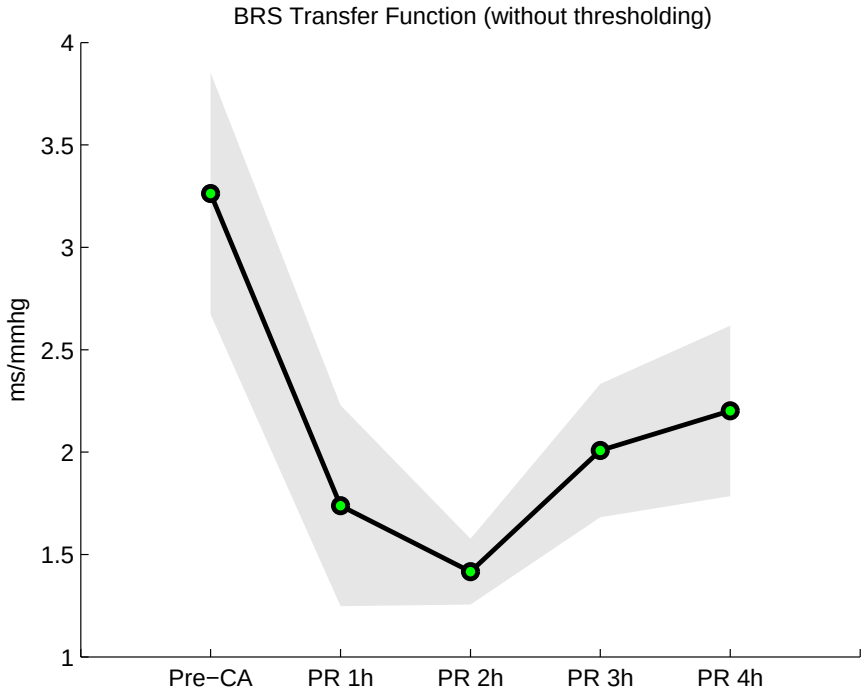

(c)

Figure 3.6: The average values of BRS in LF band, with the three different methods, are reported in the different experimental epochs. Panel (a) refers to α_{PR}, panel (b) to $\alpha_{SAP \to RR}$ and panel (c) to α_{CS}, all estimated without applying a threshold on the cross-spectrum.

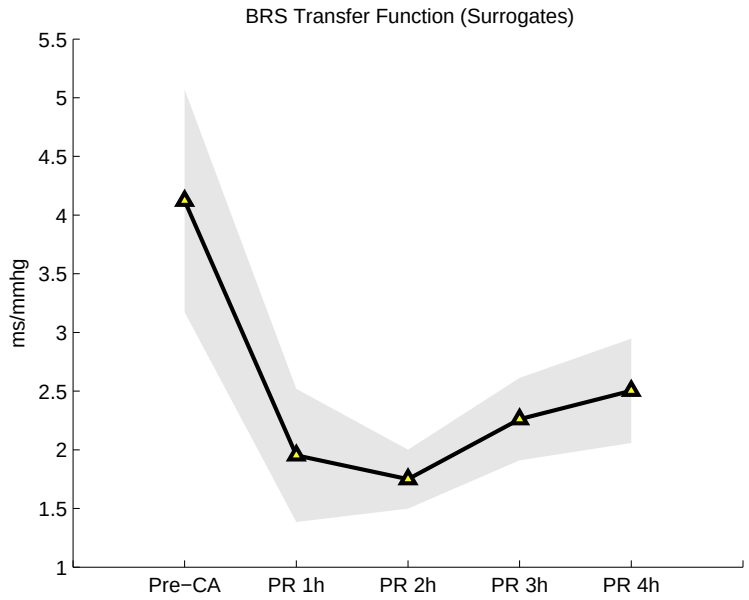

(a)

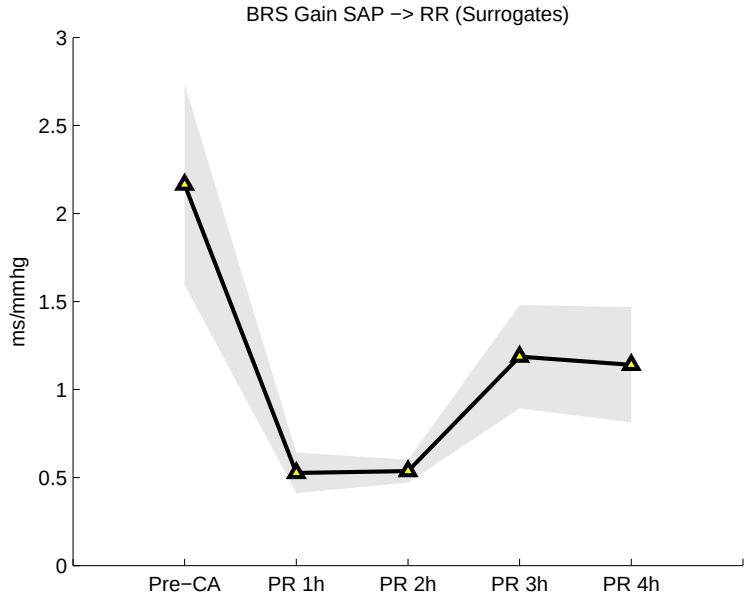

(b)

Figure 3.7: The average values of BRS gain in LF band, computed with the surrogates method, are plotted for the different experimental epochs. The gray region represent the SE interval around the mean values. Panel (a) refers to α_{CS} *and panel (b) to* $\alpha_{SAP \to RR}$.

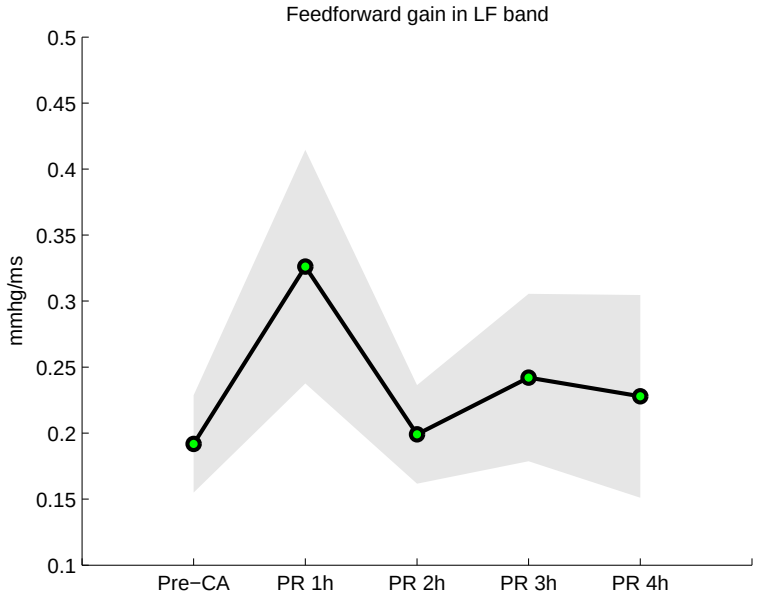

(a)

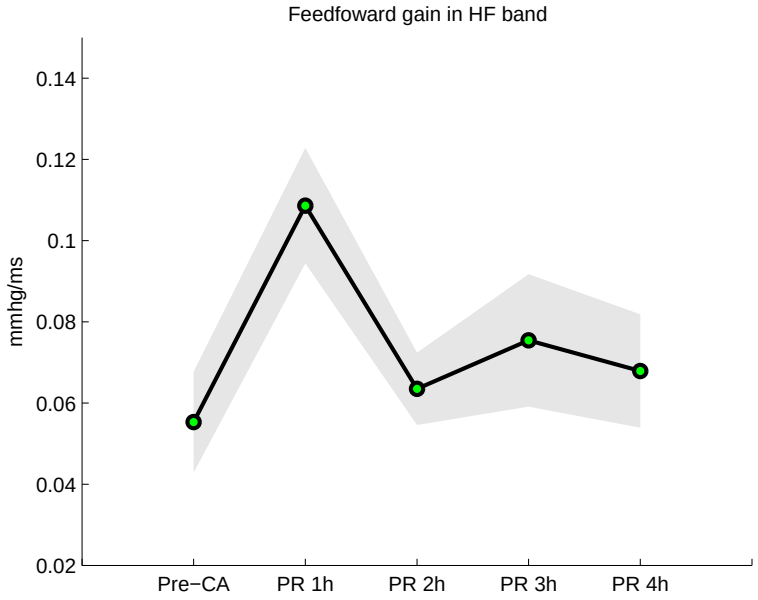

(b)

Figure 3.8: The average values of $\beta_{RR\rightarrow SAP}$ are plotted for the different experimental epochs. The gray region represent the SE interval around the mean values. Panel (a) refers to LF band and panel (b) to HF band. The method here reported does not apply a threshold to the coherence associated.

3.1.5 Impulse responses parameters

The results with the impulse response analysis are reported in Table 3.9. The *arterial baroreflex response* (ABR) magnitude is significantly lower in the post resuscitation period with respect to Pre-CA epoch, and a constant reduced ABR is maintained up to Pr 4h. The average magnitude through the different experimental epochs is reported in Figure 3.9. Another interesting result is the reduction of the average ABR peek delay through the different experimental epochs, as reported in Table 3.9 and in Figure 3.9. It is important to notice that although not significant at Pr 4h the peek delay is lower on average than the previous epochs.

Impulse response parameters	Pre-CA	Pr 1h	Pr 2h	Pr 3h	Pr 4h	RM ANOVA
ABR magnitude $ms/mmhg$	2.774±2.21	0.934±0.71 §	0.984±0.53 §	0.894±0.72 §	0.814±0.57 §	$p \leq 0.05$
ABR delay s	0.80±0.56	0.69±0.28	0.68±0.46	0.77±0.43	0.54±0.14	$n.s$

Table 3.9: The impulse response parameters expressed as mean±SD are reported in each experimental phase. The last column shows the p-value of the repeated measures *ANOVA. The symbols §,‡,# represent significant post-hoc comparisons vs Pre-CA, Pr 1h, Pr 2h, respectively.*

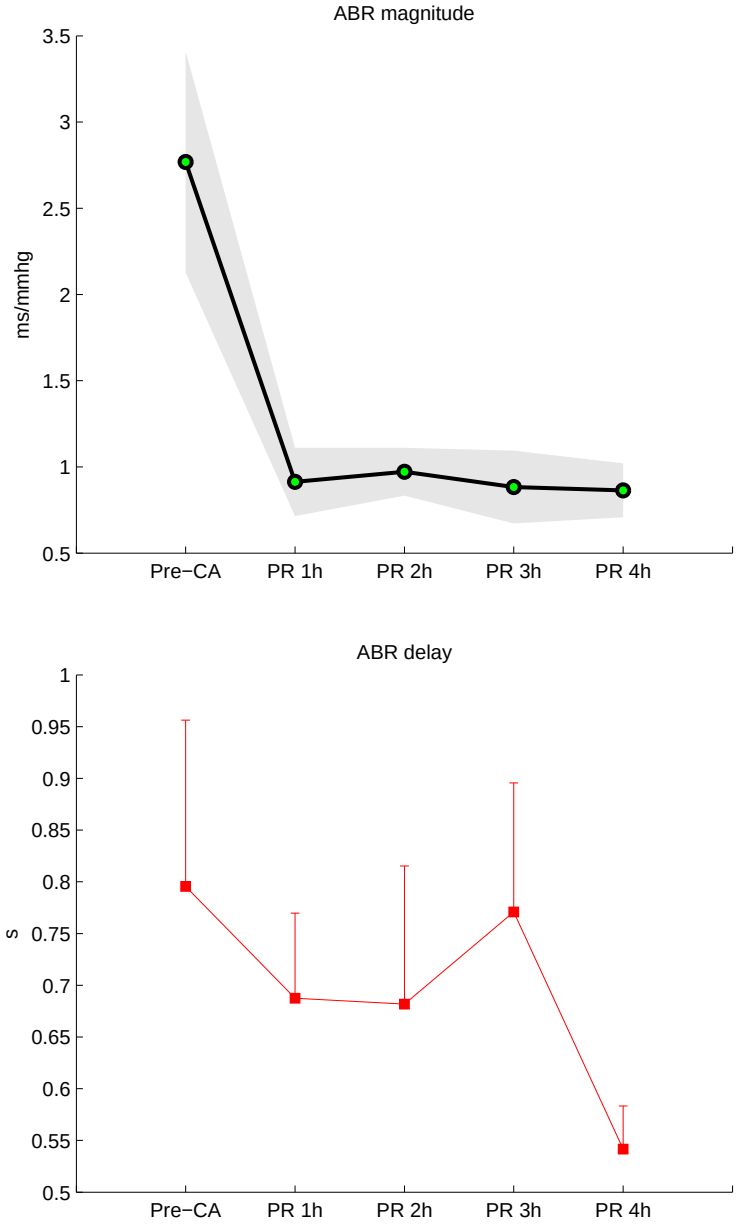

Figure 3.9: In the upper panel, the average peek-to-peek magnitude of $h_{ABR}(m)$ is reported in the different experimental epochs. The gray region represents the SE interval around the mean values. In the lower panel, the average peek delay (lower panel) of $h_{ABR}(m)$ is reported as mean+SE in the different experimental epochs.

3.2 Comparisons between argon and control groups

The results obtained are similar to the findings obtained by considering all the pigs. Indeed, the PP and the RR values do not recover. In contrast, SAP and DAP values show a recovery to levels similar to those of the Pre CA as highlighted in Table 3.10. The RR power in HF band as well as in the total power tends to recover in both groups. The baroreflex gains decrease in all the estimators considered in this study and tend to be restored in the last hours of the experiment in both groups. Table 3.10 reports only the parameters values in LF band. However there are not any significant differences between the two groups (Table 3.10 and Figure 3.10).

Groups comparisons	Pre-CA	Pr 1h	Pr 2h	Pr 3h	Pr 4h	RM ANOVA
Time-Domain Indexes						
RR mean (ms)						
Argon	603.74±169.04	455.69±148.08 §	415.43±88.58 §	444.34±106.31 §	410.38±39.66 §	$p \leq 0.01$
Control	643.59±110.20	421.24±56.72 §	457.59±55.23 §	476.08±104.43 §	476.36±92.37 §	$p \leq 0.01$
SAP mean ($mmhg$)						
Argon	123.96±16.30	94.22±13.13 §	108.63±15.44 ‡	109.68±20.22 ‡	114.56±17.87 ‡	$p \leq 0.01$
Control	112.12± 5.28	102.63±12.32	105.95±8.05	111.78±4.57 #	108.70±6.72 #	$n.s.$
DAP mean ($mmhg$)						
Argon	98.92±13.23	74.91±14.34 §	89.88±17.73 ‡	91.28±20.79 ‡	94.54±17.65 ‡	$p \leq 0.01$
Control	90.56±6.44	84.69±13.69	90.13±7.62	95.02±4.53 #	92.93±8.57 #	$n.s.$
PP mean ($mmhg$)						
Argon	25.11±5.00	19.08±4.17 §	18.90±3.99 §	18.47±3.91 §	19.90±2.98 §	$p \leq 0.01$
Control	21.54±2.32	17.98±2.17	15.77±2.45 § ‡	16.88±4.32 § ‡	15.70±2.84 § ‡	$p \leq 0.01$
PP mean ($mmhg$)						
Frequency domain indexes						
RR Power(HF) (ms^2)						
Argon	15.71±19.71	2.26±2.01	2.19±1.45	4.48±4.73	4.26±3.89	$n.s.$
Control	17.03±27.28	3.13±2.11	4.74±3.22	6.67±5.52	7.68±6.85	$n.s.$
Total RR power (ms^2)						
Argon	46.74±57.23	8.64±7.96	9.92±7.29	13.68±12.49	12.61±11.76	$n.s.$
Control	42.13±41.83	8.49±4.36	15.30±8.44	18.93±13.45 ‡	21.53±15.02 ‡	$n.s.$
BRS Values						
α_{CS}(LF) ($ms/mmhg$)						
Argon	3.11±2.31	2.09±2.37	1.70±0.73	2.00±0.91	2.33±0.97	$n.s.$
Group	3.40±1.95	1.39±0.65 §	1.24±0.42	1.80±1.30 §	2.14±1.89	$p \leq 0.05$
$\alpha_{SAP \rightarrow RR}$(LF) ($ms/mmhg$)						
Argon	2.56±2.79	0.69±0.42	0.71±0.40	1.16±0.93	0.52±0.31	$n.s.$
Group	2.03±1.69	0.72±0.47	0.71±0.30	1.11±0.70	1.45±1.29	$n.s.$
BRS Values with surrogates						
α_{CS}(LF) ($ms/mmhg$)						
Argon	4.86±3.91	2.42±2.74	1.97±1.09	2.61±1.16	2.62±1.21 #	$n.s.$
Group	3.24±2.48	1.49±0.69	1.48±0.49	1.91±1.27	2.39±1.92	$p \leq 0.05$

Table 3.10: The time domain moments, spectral indexes and BRS values expressed as mean± SD and divided by groups are reported in any experimental phase. In the last column the p-value of the repeated measures *ANOVA is shown. The symbols §,‡,# represent significant post-hoc comparisons vs Pre-CA, Pr 1h, Pr 2h, respectively. Notice that no significant differences are reported between the two animal groups.*

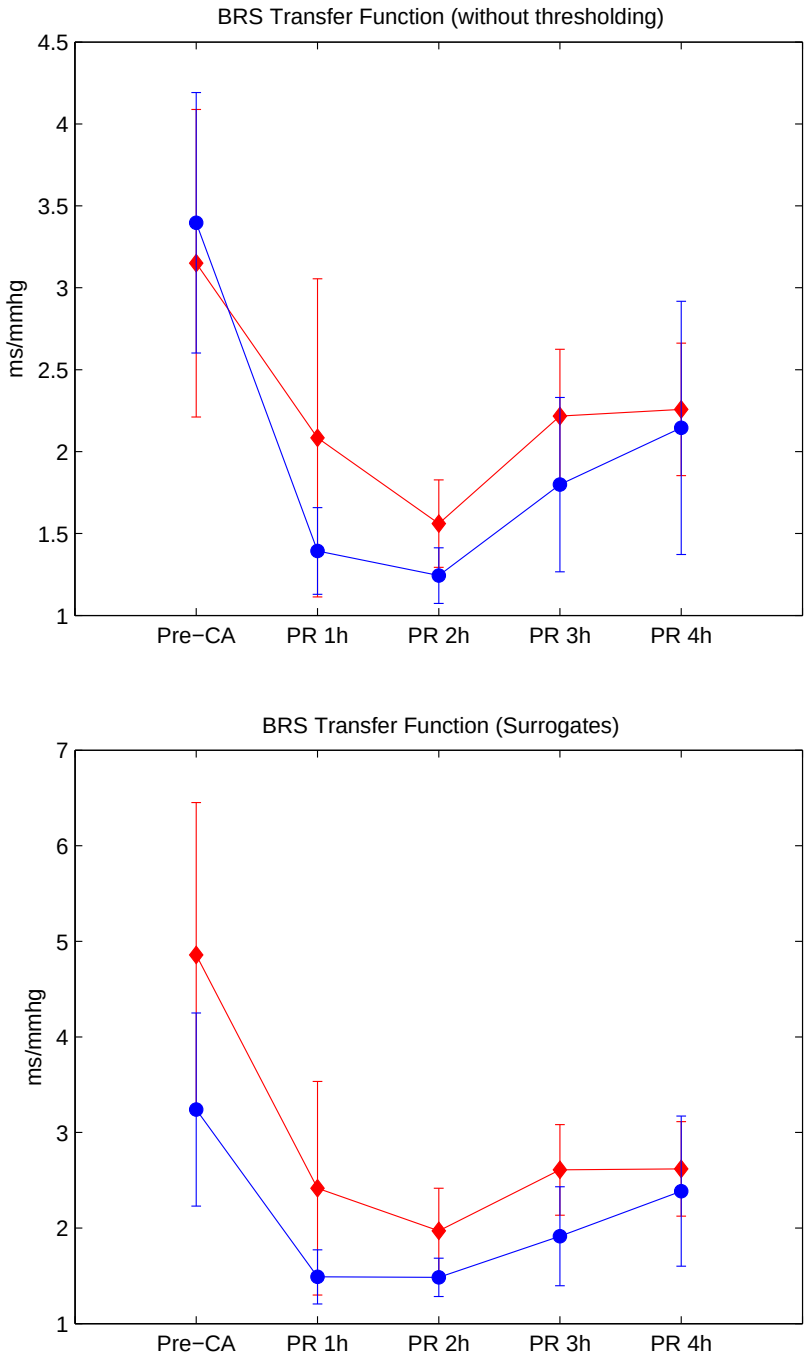

Figure 3.10: The average values of BRS in LF band, estimated with (2.3) *and divided in argon (red diamonds) and control (blue circle) groups, are reported in the different experimental epochs.*

Chapter 4

Conclusions and future research

4.1 Discussions

4.1.1 Autonomic response to cardiac arrest and baroreflex analysis

In time-domain, both RR and pressure variables averages present significantly changes during the experimental epochs. Furthermore, RR and PP do not recover after CA and their values are significantly lower with respect to the values measures before the event. In contrast, SAP and DAP increase with time course of the experiment, i.e. after resuscitation. The absolute RR power in LF band shows a decreasing trend after CA and the values in the following resuscitation period suggest a recovery, even though they are not significant. Similarly, the absolute PP power in LF band show a drop after CA without recovery. In similar way, LF components of SAP and DAP suggest a u shape in the observed time period. Interestingly, RR total power diminishes after the onset of the impairing condition and recovers in the following post resuscitation epochs.

The mechanical ventilation represents a strong driven on cardiovascular oscillations both on arterial blood pressure and on RR intervals and thus the main source of power in the HF band. This experimental condition is the principal cause of higher normalized HF power than the values commonly measured in spontaneous respiration (Table 3.3). The experimental procedure required adjustments during the observational period after CA and sometimes the respiratory rate was close to the LF band: this could be

the reason of the high variance in the LF and HF power values.

The results from the Granger causality test supports the hypothesis of a preserved ANS control on the heart rate and circulation although impaired and these results foster the successive BRS analyses. Interestingly, almost all the animals pass the test on the causality of SAP changes on RR intervals oscillations, i.e. feedback relationship, but much less animals pass the test for the feedforward mechanism, i.e. the effects of RR changes on the SAP oscillations. This can be explained by a reduced SV after CA, supported by a significant decrease in PP, and thus a reduction of the runoff effects on arterial blood pressure.

All the estimators adopted in this study show a significant decrease of the baroreflex after cardiac arrest (CA). However, a partial recovery is obtained in the last hours of post resuscitation (Figure 3.6 and Figure 3.7). There are two possible explanations to this u shape trend.

The first one is the electrical instability of the organ effector, as in the *closed loop* system the regulation of ABP through CO is mediated by the heart functioning. This hypothesis would explain also the decrease in the RR interval values, the increase of $COSEn$ values in the post resuscitation epochs and the low levels of $k^2_{RR \rightarrow SAP}$. The impaired condition of the cardiac pump may cause and at the same time be affected by inability of heart rate to contribute in maintaining blood pressure. This hypothesis is in line with trend obtained with the bivariate $\beta_{RR \rightarrow SAP}$ index: the increase of this in the first hour of post-resuscitation supports the hypothesis of a compensatory mechanism of tachycardia and consequently increase of the runoff effect.

A second hypothesis is the large reduction of the vagal control. Even though the mechanical ventilation influences the HF oscillations of the RR series, the Figure 3.3 shows a recovery after a drop after CA. The reduction of vagal stimulation and its recovery are the hypothesized main drivers of the BRS variations, according to the findings reported in the introduction of this work. Furthermore, a depression of PNS control represents a reduction of protection from cardiac arrhythmia, such as VF, as described by [31], [32]. Our results supports the findings about vagal influence on the heart, but it sheds a further light on the short-term ABP regulation. Indeed, the most likely explanation is that parasympathetic stimulation facilitates the partial BRS recovery since the same HF power partially recovers. In the post

resuscitation period, the arterial blood pressure improves, as demonstrated by the increase of SAP and DAP. However, a restoration of heart rate and cardiac electrical stability are supposed to be pivotal for an effective functioning of the baroreflex. A longer observational window should have permitted to investigate this and to verify if a complete recovery of BRS would occur.

The impulse response analyses allows to investigate how the baroreflex changes not only in terms of gain but also in terms of temporal dynamics. The ABR delay reduces after CA and is significantly shorter at Pr 4h. This finding could be interpreted as a compensation mechanism to a baroreflex gain reduction: a faster response but less large.

The partial recovery of baroreflex function could be thus seen by two perspectives: a recovery in dynamic gain (Table 3.5) and a reduction in time response, as shown by the impulse response analysis.

4.1.2 Comparison between Argon and control groups

The comparisons between the two groups do not suggest any particular difference between them. The analyses confirms the trends previously obtained by considering all the animals as an individual group. The simple clinical implication is that Argon should be used because it has been demonstrated to be neuroprotective [5] and it does not affect or reduce the impairing of the cardiovascular ANS control after the cardiac arrest.

4.2 Limitations and Further developments.

As this thesis draws to a close, inevitably there are research tasks not accomplished but would be plausible extensions of this thesis. There are also interesting research tangents to embark on.

ECG signal and measures problems. The first strong limit is the use of the HP surrogate instead of the actual RR interval. Although, in general, the presence of the mechanical delay should not influence the peak time interval identification, the individual heart cycle of ABP and its time occurrence could be distorted by nonlinear phenomenon that difficulty can be quantified. These factors could make HP differ from RR. However, this choice is actually a consequence of the bad quality of ECG signal. Some QRS detection algorithms have been tested to detect the R-peak, but they are

actually confounded by the noise on the ECG and by a large ST deviation. In fact, due to the OCA, the signals show an ST elevation, accompanied by a large T wave whose extent is comparable with R peak. The automatic classification algorithm frequently confounds the T wave with R peak, introducing a fake variability in RR series. A proper algorithm should be developed to this task.

Furthermore, the ABP waveform is affected by noises as well, mainly due to measurement procedure. For example, sharpen and sudden reductions in pressure amplitude as well as dicrotic notch, whose extent is comparable to the systolic peak, may be due to a misplacement of the catheter. In similar way to ECG, there are factors which make impossible to extract SAP and DAP series, but they were less frequent than ECG problems.

Stationarity test. The stationarity of the time series is an important requirement for a reliable estimation of the spectral analysis and BRS estimation. The inclusion of a proper test in order to verify it would strengthen this type of analysis.

Future experiments. The current experiment is actually designed for a different task than the baroreflex analysis. Signal quality apart, four hours of post-resuscitation only is the main limitations of this study. It would be interesting to study the cardiovascular regulation in a longer time window, in order to verify the recovery of BRS and its association to other cardiovascular parameters. Furthermore, a specific protocol to inhibit or stimulate vagal discharge on cardiac activity could confirm that BRS variations after CA is driven by parasympathetic stimulation.

4.3 Conclusions

The present study investigates the BRS by means of different methods for each experimental different epoch after CA and these analyses confirm the presence of a partial recovery in the post resuscitation period. The argon has not any role to protect or preserve the baroreflex after CA or during PR and, in general, the autonomous nervous system functions. Finally, spectral and non linear analyses and impulse response investigation draw attention to some mechanism which develop after CA. On one hand, a recovery of the vagal stimulation with a faster dynamics of baroreflex drives the baroreflex recovery and, on the other, this trend towards a normal functioning could

be enhanced by a reduction of cardiac electric instability, which remains sustained in post-resuscitation.

Bibliography

[1] A. Porta, G. Baselli, and S. Cerutti. Implicit and Explicit Model-Based Signal Processing for the Analysis of Short-Term Cardiovascular Interactions. *Proceedings of the IEEE*, 94(4):805–818, 2006.

[2] G. Baselli, S. Cerutti, S. Civardi, a. Malliani, and M. Pagani. Cardiovascular variability signals: Towards the identification of a closed-loop model of the neural control mechanisms. *IEEE Transactions on Biomedical Engineering*, 35(12):1033–1046, 1988.

[3] Riccardo Barbieri, John K Triedman, and J Philip Saul. Heart rate control and mechanical cardiopulmonary coupling to assess central volume: a systems analysis. *American journal of physiology. Regulatory, integrative and comparative physiology*, 283:R1210–R1220, 2002.

[4] Jan-Thorsten Gräsner and Leo Bossaert. Epidemiology and management of cardiac arrest: what registries are revealing. *Best practice & research. Clinical anaesthesiology*, 27(3):293–306, 2013.

[5] Giuseppe Ristagno, Francesca Fumagalli, Ilaria Russo, Simona Tantillo, Davide Danilo Zani, Valentina Locatelli, Marcella De Maglie, Deborah Novelli, Lidia Staszewsky, Tarcisio Vago, Angelo Belloli, Mauro Di Giancamillo, Roberto Fries, Michael Fries, Serge Masson, Eugenio Scanziani, and Roberto Latini. Postresuscitation treatment with argon improves early neurological recovery in a porcine model of cardiac arrest. *Shock*, 41(1):72–78, 2014.

[6] Gaetano M De Ferrari, Antonio Sanzo, Grazia Maria Castelli, Annalisa Turco, Alice Ravera, Fabio Badilini, and Peter J Schwartz. Rapid Recovery of Baroreceptor Reflexes in Acute Myocardial Infarction is a Marker of Effective Tissue Reperfusion. *Journal of cardiovascular translational research*, pages 553–559, 2014.

[7] Dee Unglaub Silverthorn. *Human Physiology: An Integrated Approach*. Pearson Education, 2015.

[8] Arthur C. Guyton and John E. Hall. *Textbook of Medical Physiology.* Elsevier Health Sciences, 2006.

[9] Patrice G. Guyenet. The sympathetic control of blood pressure. *Nature Reviews Neuroscience*, 7(5):335–346, 2006.

[10] Guadalupe Dorantes Mendez. Dynamic cardiovascular control of arterial blood pressure and heart rate in response to central volume variations and anesthesia . *PhD thesis. Politecnico di Milano*, 2013.

[11] Mark W. Chapleau, Zhi Li, Silvana S. Meyrelles, Xiuying Ma, and François M. Abboud. Mechanisms determining sensitivity of baroreceptor afferents in health and disease. *Annals of the New York Academy of Sciences*, 940(1):1–19, 2001.

[12] Roy Freeman. Assessment of cardiovascular autonomic function. *Clinical Neurophysiology*, 117(4):716–730, 2006.

[13] T. H. Desai, J. C. Collins, M. Snell, and R. Mosqueda-Garcia. Modeling of arterial and cardiopulmonary baroreflex control of heart rate. *Am J Physiol Heart Circ Physiol*, 272(5):H2343–2352, may 1997.

[14] S. F. Vatner and M. Zimpfer. Bainbridge reflex in conscious, unrestrained, and tranquilized baboons. *Am J Physiol Heart Circ Physiol*, 240(2):H164–167, feb 1981.

[15] R G O'Regan and S Majcherczyk. Role of peripheral chemoreceptors and central chemosensitivity in the regulation of respiration and circulation. *The Journal of experimental biology*, 100:23–40, 1982.

[16] William K. Milsom and Mark L. Burleson. Peripheral arterial chemoreceptors and the evolution of the carotid body. *Respiratory Physiology & Neurobiology*, 157(1):4–11, 2007.

[17] Eugene Nattie and Aihua Li. Central chemoreception 2005: A brief review. *Autonomic Neuroscience*, 126-127:332–338, 2006.

[18] Sukhamay Lahiri and Robert E. Forster. CO2/H+ sensing: Peripheral and central chemoreception. *International Journal of Biochemistry and Cell Biology*, 35(10):1413–1435, 2003.

[19] John R Halliwill, Barbara J Morgan, and Nisha Charkoudian. Peripheral chemoreflex and baroreflex interactions in cardiovascular regulation in humans. *The Journal of physiology*, 552:295–302, 2003.

[20] V K Somers, a L Mark, and F M Abboud. Interaction of baroreceptor and chemoreceptor reflex control of sympathetic nerve activity in normal humans. *The Journal of clinical investigation*, 87(6):1953–1957, 1991.

[21] HP Koepchen. History of studies and concepts of blood pressure waves. *Mechanisms of blood pressure waves*, pages 3–23, 1984.

[22] M T La Rovere, J T Bigger, Frank I Marcus, Andrea Mortara, and Peter J Schwartz. Baroreflex sensitivity and heart-rate variability in prediction of total cardiac mortality after myocardial infarction. ATRAMI. *Lancet*, 351(9101):478–484, 1998.

[23] AJ Camm, M Malik, JT Bigger, and B Günter. Task force of the European Society of Cardiology and the North American Society of Pacing and Electrophysiology. Heart rate variability: standards of measurement, physiological interpretation and clinical use. *Circulation*, 93(5):1043–1065, 1996.

[24] Robert E. Kleiger, J.Philip Miller, J.Thomas Bigger, and Arthur J. Moss. Decreased heart rate variability and its association with increased mortality after acute myocardial infarction. *The American Journal of Cardiology*, 59(4):256–262, feb 1987.

[25] T G Farrell, Y Bashir, T Cripps, M Malik, J Poloniecki, E D Bennett, D E Ward, and a J Camm. Risk stratification for arrhythmic events in postinfarction patients based on heart rate variability, ambulatory electrocardiographic variables and the signal-averaged electrocardiogram. *Journal of the American College of Cardiology*, 18(3):687–697, 1991.

[26] J T Bigger, J L Fleiss, L M Rolnitzky, and R C Steinman. Frequency domain measures of heart period variability to assess risk late after myocardial infarction. *Journal of the American College of Cardiology*, 21(3):729–736, 1993.

[27] Peter J Vanoli, Emilio and De Ferrari, Gaetano M and Stramba-Badiale, Marco and Hull, SS and Foreman, Robert D and Schwartz. Vagal stimulation and prevention of sudden death in conscious dogs with a healed myocardial infarction. *Circulation research*, 68(5):1471–1481, 1991.

[28] M Piepoli, A J Coats, S Adamopoulos, L Bernardi, Y H Feng, J Conway, and P Sleight. Persistent peripheral vasodilation and sympathetic

activity in hypotension after maximal exercise. *Journal of applied physiology*, 75(4):1807–14, oct 1993.

[29] H S Smyth, P Sleight, and G W Pickering. Reflex regulation of arterial pressure during sleep in man. A quantitative method of assessing baroreflex sensitivity. *Circulation research*, 24(1):109–121, 1969.

[30] K E Airaksinen, K U Tahvanainen, D L Eckberg, M J Niemela, A Yli-italo, and H V Huikuri. Arterial baroreflex impairment in patients during acute coronary occlusion. *J Am Coll Cardiol*, 32(6):1641–1647, 1998.

[31] D Cerati and P J Schwartz. Single cardiac vagal fiber activity, acute myocardial ischemia, and risk for sudden death. *Circulation research*, 69(5):1389–1401, 1991.

[32] L Babai, J G Papp, J R Parratt, and A Vegh. The antiarrhythmic effects of ischaemic preconditioning in anaesthetized dogs are prevented by atropine; role of changes in baroreceptor reflex sensitivity. *Br.J.Pharmacol.*, 135(1):55–64, 2002.

[33] A Malliani, D F Peterson, V S Bishop, and A M Brown. Spinal sympathetic cardiocardiac reflexes. *Circulation research*, 30(2):158–166, 1972.

[34] Azad Ghuran, Fiona Reid, Maria Teresa La Rovere, Georg Schmidt, J.Thomas T Bigger, J Camm, Peter J Schwartz, Marek Malik, and A.John Camm. Heart rate turbulence-based predictors of fatal and nonfatal cardiac arrest (The autonomic tone and reflexes after myocardial infarction substudy). *The American Journal of Cardiology*, 89(2):184–190, 2002.

[35] H. Bonnemeier. Reflex Cardiac Activity in Ischemia and Reperfusion: Heart Rate Turbulence in Patients Undergoing Direct Percutaneous Coronary Intervention for Acute Myocardial Infarction. *Circulation*, 108(8):958–964, 2003.

[36] G Schmidt, A Bauer, P Barthel, R Schneider, and M Malik. Heart rate turbulence dynamicity. *European Heart Journal*, 22:436, 2001.

[37] Noorulhuda Jawad, Maleeha Rizvi, Jianteng Gu, Olar Adeyi, Guocai Tao, Mervyn Maze, and Daqing Ma. Neuroprotection (and lack of neuroprotection) afforded by a series of noble gases in an in vitro model of neuronal injury. *Neuroscience Letters*, 460(3):232–236, 2009.

[38] Mark Coburn, Robert D. Sanders, Daqing Ma, Michael Fries, Steffen Rex, Guy Magalon, and Rolf Rossaint. Argon. *European Journal of Anaesthesiology*, 29(12):549–551, 2012.

[39] A Brücken, A Cizen, C Fera, A Meinhardt, J Weis, K Nolte, R Rossaint, T Pufe, G Marx, and M Fries. Argon reduces neurohistopathological damage and preserves functional recovery after cardiac arrest in rats. *British Journal of Anaesthesia*, 110 Suppl(February):i106–12, 2013.

[40] G Ristagno, W Tang, T Y Xu, S Sun, and M H Weil. Outcomes of CPR in the presence of partial occlusion of left anterior descending coronary artery. *Resuscitation*, 75(2):357–365, 2007.

[41] Giuseppe Ristagno, Carlos Castillo, Wanchun Tang, Shijie Sun, Joe Bisera, and Max Harry Weil. Miniaturized mechanical chest compressor: a new option for cardiopulmonary resuscitation. *Resuscitation*, 76(2):191–7, 2008.

[42] Michael C K Khoo. Modeling of autonomic control in sleep-disordered breathing. *Cardiovascular Engineering*, 8(1):30–41, 2008.

[43] A Malliani, M Pagani, F Lombardi, and S Cerutti. Cardiovascular neural regulation explored in the frequency domain. *Circulation*, 1991.

[44] Michael C. K. Khoo. *Physiological Control Systems: Analysis, Simulation, and Estimation*. Wiley Online Library, 1999.

[45] J. P. Saul, R. D. Berger, P. Albrecht, S. P. Stein, M. H. Chen, and R. J. Cohen. Transfer function analysis of the circulation: unique insights into cardiovascular regulation. *Am J Physiol Heart Circ Physiol*, 261(4):H1231–1245, oct 1991.

[46] Sergio Cerutti, Giuseppe Baselli, Anna Bianchi, Enrico Caiani, Davide Contini, Rinaldo Cubeddu, Fabio Dercole, Luca Rienzo, Diego Liberati, Luca Mainardi, Paolo Ravazzani, Sergio Rinaldi, Maria Signorini, and Alessandro Torricelli. Biomedical signal and image processing. *IEEE pulse*, 2(3):41–54, jan 2011.

[47] AC Guyton and JP Montani. Computer models for designing hypertension experiments and studying concepts. *The American journal of the medical sciences*, 295(4):320—-326, 1988.

[48] R Barbieri, G Parati, and J P Saul. Closed- versus open-loop assessment of heart rate baroreflex. *IEEE engineering in medicine and biology magazine*, 20(2):33–42, 2001.

[49] Eberhard von Borell, Jan Langbein, Gérard Després, Sven Hansen, Christine Leterrier, Jeremy Marchant-Forde, Ruth Marchant-Forde, Michela Minero, Elmar Mohr, Armelle Prunier, Dorothée Valance, and Isabelle Veissier. Heart rate variability as a measure of autonomic regulation of cardiac activity for assessing stress and welfare in farm animals - A review. *Physiology and Behavior*, 92(3):293–316, 2007.

[50] S M Horner, C F Murphy, B Coen, D J Dick, F G Harrison, Z Vespalcova, and M J Lab. Contribution to heart rate variability by mechanoelectric feedback. Stretch of the sinoatrial node reduces heart rate variability. *Circulation*, 94(7):1762–1767, 1996.

[51] RW De Boer, JM Karemaker, and J Strackee. Relationships between short-term blood-pressure fluctuations and heart-rate variability in resting subjects I: a spectral analysis approach. *Medical and Biological Engineering and Computing*, 23(4):352–358, 1985.

[52] H. W. Robbe, L. J. Mulder, H. Ruddel, W. A. Langewitz, J. B. Veldman, and G. Mulder. Assessment of baroreceptor reflex sensitivity by means of spectral analysis. *Hypertension*, 10(5):538–543, nov 1987.

[53] G Mancia, G Parati, P Castiglioni, and M di Rienzo. Effect of sinoaortic denervation on frequency-domain estimates of baroreflex sensitivity in conscious cats. *The American journal of physiology*, 276(6 Pt 2):H1987–93, jun 1999.

[54] Giandomenico Nollo, Alberto Porta, Luca Faes, Maurizio Del Greco, Marcello Disertori, and Flavia Ravelli. Causal linear parametric model for baroreflex gain assessment in patients with recent myocardial infarction. *Am J Physiol Heart Circ Physiol*, 280(4):H1830–1839, apr 2001.

[55] Andrea Mortara, Maria Teresa La Rovere, Gian Domenico Pinna, Paolo Parziale, Roberto Maestri, Soccorso Capomolla, Cristina Opasich, Franco Cobelli, and Luigi Tavazzi. Depressed arterial baroreflex sensitivity and not reduced heart rate variability identifies patients with chronic heart failure and nonsustained ventricular tachycardia: The effect of high ventricular filling pressure. *American Heart Journal*, 134(5):879–888, nov 1997.

[56] A Radaelli and S Perlangeli. Altered blood pressure variability in patients with congestive heart failure. *Journal of hypertension*, 17(12):1905—-1910, 1999.

[57] GD Pinna and R Maestri. Reliability of transfer function estimates in cardiovascular variability analysis. *Medical and Biological Engineering and Computing*, 2001.

[58] Luca Faes, Gian Domenico Pinna, Alberto Porta, Roberto Maestri, and Giandomenico Nollo. Surrogate data analysis for assessing the significance of the coherence function. *IEEE Transactions on Biomedical Engineering*, 51(7):1156–1166, 2004.

[59] G D Pinna and R Maestri. New criteria for estimating baroreflex sensitivity using the transfer function method. *Medical & biological engineering & computing*, 40(1):79–84, 2002.

[60] G Van Belle, LD Fisher, PJ Heagerty, and T Lumley. *Biostatistics: a methodology for the health sciences*. John Wiley & Sons, 2004.

[61] J Theiler, S Eubank, and A Longtin. Testing for nonlinearity in time series: the method of surrogate data. *Physica D: Nonlinear Phenomena*, 58(1):77–94, 1992.

[62] Thomas Schreiber and Andreas Schmitz. Surrogate time series. *Physica D: Nonlinear Phenomena*, 142(3-4):346–382, 2000.

[63] Vegard Bruun Wyller, Riccardo Barbieri, and J Philip Saul. Blood pressure variability and closed-loop baroreflex assessment in adolescent chronic fatigue syndrome during supine rest and orthostatic stress. *European journal of applied physiology*, 111(3):497–507, 2011.

[64] a. Porta, R. Furlan, O. Rimoldi, M. Pagani, a. Malliani, and P. Van De Borne. Quantifying the strength of the linear causal coupling in closed loop interacting cardiovascular variability signals. *Biological Cybernetics*, 86(3):241–251, 2002.

[65] RA Wiggins and EA Robinson. Recursive solution to the multichannel filtering problem. *Journal of Geophysical Research*, 1965.

[66] T Söderström and P Stoica. *System identification*. Prentice-Hall, Inc., 1988.

[67] Tito Bassani, Valentina Magagnin, Stefano Guzzetti, Giuseppe Baselli, Giuseppe Citerio, and Alberto Porta. Testing the involvement of baroreflex during general anesthesia through Granger causality approach. *Computers in biology and medicine*, 42(3):306–12, 2012.

[68] V Z Marmarelis. Identification of nonlinear biological systems using Laguerre expansions of kernels. *Annals of Biomedical Engineering*, 21(6):573–589, 1993.

[69] Ed Joseph D Bronzino. Chapter 163 - Methods and Tools for Identification of Physiologic Systems. *Biomedical Engineering*, 2000.

[70] S Cerutti and C Marchesi. *Advanced methods of biomedical signal processing*. John Wiley & Sons, 2011.

[71] J S Richman and J R Moorman. Physiological time-series analysis using approximate entropy and sample entropy. *American journal of physiology. Heart and circulatory physiology*, 278(6):H2039–H2049, 2000.

[72] Douglas E Lake, Joshua S Richman, M Pamela Griffin, and J Randall Moorman. Sample entropy analysis of neonatal heart rate variability. *American journal of physiology. Regulatory, integrative and comparative physiology*, 283(3):R789–R797, 2002.

[73] Madalena D. Costa, Chung-Kang Peng, and Ary L. Goldberger. Multiscale Analysis of Heart Rate Dynamics: Entropy and Time Irreversibility Measures. *Cardiovascular Engineering*, 8(2):88–93, 2008.

[74] Douglas E Lake and J Randall Moorman. Accurate estimation of entropy in very short physiological time series: the problem of atrial fibrillation detection in implanted ventricular devices. *American journal of physiology. Heart and circulatory physiology*, 300(1):H319–H325, 2011.

[75] Claude Elwood Shannon. A mathematical theory of communication. *ACM SIGMOBILE Mobile Computing and Communications Review*, 5(1):3–55, 2001.

[76] AN Kolmogorov. A new metric invariant of transient dynamical systems and automorphisms in Lebesgue spaces. *Dokl. Akad. Nauk SSSR (NS)*, 1958.

[77] AN Kolmogorov. Entropy per unit time as a metric invariant of automorphisms. *Dokl. Akad. Nauk SSSR*, 1959.

[78] SM Pincus. Approximate entropy as a measure of system complexity. *Proceedings of the National Academy of Sciences*, 88(6):2297–2301, 1991.

[79] TJ Moss, DE Lake, and JR Moorman. Local dynamics of heart rate: detection and prognostic implications. *Physiological measurement*, 2014.

[80] W. Zong, T. Heldt, G.B. Moody, and R.G. Mark. An open-source algorithm to detect onset of arterial blood pressure pulses. *Computers in Cardiology, 2003*, pages 259–262, 2003.

[81] Niels Wessel, Andreas Voss, Hagen Malberg, Christine Ziehmann, Henning U. Voss, Alexander Schirdewan, Udo Meyerfeldt, and Jürgen Kurths. Nonlinear analysis of complex phenomena in cardiological data. *Herzschrittmachertherapie und Elektrophysiologie*, 11(3):159–173, oct 2000.

[82] Travis J Moss, Douglas E Lake, and J Randall Moorman. Local dynamics of heart rate: detection and prognostic implications. *Physiological Measurement*, 35:1929–1942, 2014.

[83] Thomas Schreiber. Constrained Randomization of Time Series Data. *Physical Review Letters*, 80(10):2105–2108, mar 1998.

[84] Rainer Hegger, Holger Kantz, and Thomas Schreiber. Practical implementation of nonlinear time series methods: The TISEAN package. *Chaos: An Interdisciplinary Journal of Nonlinear Science*, 9(2):413–435, jun 1999.

[85] H. Raymundo, A. M. Scher, D. S. O'Leary, and P. D. Sampson. Cardiovascular control by arterial and cardiopulmonary baroreceptors in awake dogs with atrioventricular block. *Am J Physiol Heart Circ Physiol*, 257(6):H2048–2058, dec 1989.

[86] Anna Blasi, Javier Antonio Jo, Edwin Valladares, Ricardo Juarez, Ahmet Baydur, and Michael C K Khoo. Autonomic cardiovascular control following transient arousal from sleep: a time-varying closed-loop model. *IEEE Transactions on Biomedical Engineering*, 53(1):74–82, 2006.